

# New Physics of Dipole and Quadrupole Brewster Angles in Thin Films

Edward H.Krock<sup>1\*</sup>, Mughaid Ali<sup>1</sup>, Haizhong Weng<sup>1</sup>,  
C. M. Smith<sup>1</sup>, John F.Donegan<sup>1\*</sup>

<sup>1</sup>School of Physics, CRANN, and AMBER, Trinity College Dublin,  
Dublin 2, Ireland.

\*Corresponding author(s). E-mail(s): [ekrock@tcd.ie](mailto:ekrock@tcd.ie); [jdonegan@tcd.ie](mailto:jdonegan@tcd.ie);

## Abstract

The Brewster angle is a well-known phenomenon that describes the angle dependent reflection minimum resulting from the difference in the refractive index between two media for p-polarized light. From multipole decomposition, we show this well-known Brewster angle for the electric dipole term, but also new Brewster angles for the magnetic dipole, electric quadrupole, and magnetic quadrupole terms for p-and s-polarizations. Our new equations show that the complex dipole and quadrupole moments must become real valued for the Brewster angle to occur. After applying our new theory to the reflection of a thin-dielectric SiN film, we identify a previously undiscovered interference effect required to observe the Brewster angle in thin films, the destructive interference between magnetic dipole and electric quadrupole terms. The electric dipole Brewster angle occurs for all wavelengths studied but those of the magnetic dipole, electric quadrupole and magnetic quadrupole occur over a very narrow wavelength range.

## 1 Introduction

In 1815 [1] David Brewster observed a simple law for the angle of incidence at which an unpolarized incident beam is perfectly s-polarized upon reflection from a dielectric medium with refractive index  $n$ .

$$\tan(\theta_B) = n \quad (1)$$

This leads to the current macroscopic understanding of the Brewster angle illustrated in Figure 1. The Brewster angle occurs when the angle of incidence aligns with the electric dipole moment of the medium which will result in the reflected ray being perfectly s-polarized.

In more modern-day usage, a zero in reflected intensity is generally considered to occur at the Brewster angle

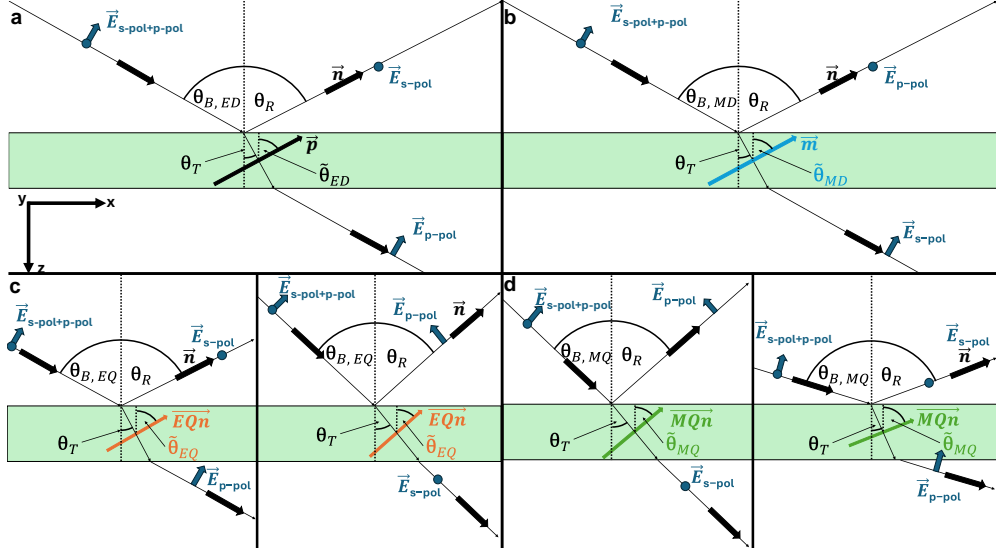


**Fig. 1** Illustration of geometry for incident (s- and p-polarized), reflected and transmitted electric fields from a thin film considering each multipole on its own. Subplot (a) illustrates the traditional Brewster angle, the electric dipole moment,  $\vec{p}$ , aligns with the reflected ray,  $\vec{n}$ , and the reflected ray is perfectly s-polarized. However, the Brewster angle can be observed for all multipoles as we show below, as any multipole moment may align with the reflected ray. Subplots (b) illustrate this for the magnetic dipole, where the reflected ray is perfectly p-polarized. Subplots (c)-(d) illustrate this for the electric/ magnetic quadrupoles, where the reflected ray may be perfectly s- or p-polarized depending on the direction of the incident ray. Brewster angles are denoted with various subscripts e.g. MD and complex multipoles are also indicated

[2]. In the past decade, this picture has been further broadened to what is termed a generalized Brewster angle effect [3–6]. In these studies, the alignment of angle of incidence and electric dipole moment is not identified directly, but a zero reflection/polarizing angle is identified. Through the use of metamaterials or optical absorbing layers, the generalized Brewster angle effect can be observed for both s- and p-polarized incident light. Thus, zero reflection can be engineered at multiple wavelengths and at multiple angles of incidence.

Interpreting reflection in optical metamaterials has been well developed, where multipole decomposition can describe this reflection in terms of electric and magnetic multipoles [7, 8]. This

methodology is vital in the understanding of a variety of phenomena, including toroidal multipoles [10], as these play a role in the observation of anapoles [11–13]. Other interference phenomena such as Kerker effects, the interference between electric and magnetic multipoles [14–16] also occur with metamaterials. The presence of magnetic multipoles at frequencies where the bulk permeability of materials is unity [9, 17] is known as “Optical Magnetism”, [7, 9, 18] which enables metamaterials to support unusual phenomena such as negative refraction [19] and transverse electric surface waves [20].

Our work here shows that this generalized Brewster angle effect does not require the use of metamaterials but is a fundamental aspect of reflection from

dielectric thin films. We proceed through the use of multipole decomposition to explain how light is reflected from such a simple homogeneous material. To our knowledge, only a single modeling study on thin films has been performed to date, which involved a subwavelength film of 200 nm GaP studied at normal incidence [21]. They demonstrated that Fabry Perot modes arise from the interference between electric and magnetic multipoles, showing that optical magnetism is not unique to metamaterials. However, combined experimental evidence and theoretical interpretation of angle dependent behavior has not been explored, and is the focus of this work.

We demonstrate that the Brewster angle equation, one of the best known in Physics, not only applies to the electric dipole (Figure 1 (a)) but the magnetic dipole, electric quadrupole and magnetic quadrupoles as illustrated in Figure 1 (b)-(d). For the standard Brewster angle, we find that in addition to the alignment of the electric dipole with the angle of incidence, the magnetic dipole and electric quadrupole destructively interfere to produce the observed zero in reflection. The alignment between the angle of incidence and electric dipole is typically considered in the real plane, however we demonstrate that multipole analysis produces complex angles and so this alignment must be considered in the real and imaginary planes.

Our work broadens and completes the understanding of Brewster angles and its relation to the polarization response of thin film dielectrics, and offers exciting opportunities to realize new Brewster angle physics in future devices.

## 2 Multipole Theory of Brewster Angles

Multipole decomposition describes the complex reflection coefficient,  $r$ , from a dielectric thin film in terms of electric and magnetic multipoles with equation 2.

These multipole moments are shown in the expected order of their contribution to the overall reflection, which are the electric dipole (ED), magnetic dipole (MD), electric quadrupole (EQ), magnetic quadrupole (MQ), electric octupole (EO) and magnetic octupoles (MO). Our model extends this behavior to all angle of incidence, implementation of this model is explained in the methods section, and it's derivation is in the supplemental material, S2.

$$\begin{aligned}
 r = & \frac{ik_d}{E_0 2S_L \epsilon_0 \epsilon_d} [\vec{n} \times (\vec{p} \times \vec{n})] + \frac{1}{v_d} [\vec{m} \times \vec{n}] \\
 & + \frac{ik_d}{6} [\vec{n} \times (\vec{n} \times \hat{Q}\vec{n})] + \frac{ik_d}{2v_d} [\vec{n} \times \vec{M}\vec{n}] \\
 & + \frac{k_d^2}{6} [\vec{n} \times [\vec{n} \times \hat{O}^e \vec{n}\vec{n}]] + \frac{k_d^2}{6v_d} [\vec{n} \times \hat{O}^m \vec{n}\vec{n}]
 \end{aligned} \tag{2}$$

Figure 1 illustrates our Brewster angles and includes several additional angles,  $\theta_B$  describes the angle of incidence that the Brewster angle occurs at. Angles of incidence  $\theta_I$ , transmission  $\theta_T$  and angle of reflection  $\theta_R$  are well known. Each multipole will have its own Brewster angle which we denote for electric dipole  $\theta_{B,ED}$ . In addition, each multipole has its own angle,  $\theta_{ED}, \theta_{MD}, \theta_{EQ}, \theta_{MQ}$  that are in general complex.

In our analysis of reflection and transmission of light from a thin film, we begin by considering each of the terms in equation 2 on their own. Later we

will look at their combined effects in the model and in experiment.

We first derive the Brewster angle arising from the electric dipole. In equation 2, the resulting cross products between  $\vec{n}$  and  $\vec{p}$  leads to the following vector for the reflected light. The zero-reflection case which we expect at the Brewster angle should correspond to when,  $\vec{n}$  and  $\vec{p}$  are parallel or align, which agrees with the macroscopic description of the Brewster angle. We note that the  $\vec{p}$  is typically a complex vector given the electric field is itself complex and hence the multipole angles calculated in the multipole analysis are complex in general, but we will show that at the Brewster angle, the complex electric dipole moment becomes a real vector. From the first term in equation 2,  $\vec{n} \times (\vec{p} \times \vec{n})$ , we have the following vector for reflection from an electric dipole.

$$\begin{bmatrix} \cos(\theta_I)(p_x \cos(\theta_I) - p_z \sin(\theta_I)) \\ p_y \\ \sin(\theta_I)(p_z \sin(\theta_I) - p_x \cos(\theta_I)) \end{bmatrix} \quad (3)$$

The first/third element of this vector describes to p-polarized light, the second element describes s-polarized light, and has no angle dependence. Therefore, the electric dipole supports a single p-polarized Brewster angle. Setting this equal to zero, gives us equation 4.

$$\cos(\theta_I)(p_x \cos(\theta_I) - p_z \sin(\theta_I)) = 0 \quad (4)$$

Making the angle of incidence equal to the Brewster angle,  $\theta_I = \theta_{B,ED}$  and simplification of equation 4 results in the following condition.

$$\tan(\theta_{B,ED}) = \frac{p_x}{p_z} = n \quad (5)$$

Equation 5 defines a condition where the electric dipole does not reflect any light, which occurs when the tangent of the angle of incidence is equal to the ratio of the complex electric dipole moment along the x- and z-directions. In order for equation 5 to be satisfied, and for the Brewster angle to occur, these moments must be real numbers. The equivalence of equation 5 and the well-known Brewster angle in equation 1 is justified in the supplemental material S2.1, where we identify the Brewster condition in equation 5.

The angle of the complex electric dipole moment is the inverse tangent of the electric dipole moment ratio in equation 5.

$$\begin{aligned} \text{atan}\left(\frac{p_x}{p_z}\right) &= \tilde{\theta}_{ED} \\ &= \theta_{ED,r} + i\theta_{ED,i} \end{aligned} \quad (6)$$

Applying the inverse tangent to equation 5, gives us a modified form of the Brewster angle condition.

$$\theta_{ED,r} - \theta_I + i\theta_{ED,i} = 0^\circ + 0i \quad (7)$$

$\theta_{ED,r}$  and  $\theta_{ED,i}$  are the real and imaginary parts of the electric dipole angle. We can now derive the angle of incidence that satisfies the Brewster angle condition for any multipole using this method. As with the electric dipole derivation, we presume that only a single multipole is contributing to reflection. The detailed derivations are available in the supplemental material, S2.2-2.4 and we only present the derived equations

For the magnetic dipole we obtain a single s-polarized condition where  $m_x$  is the magnetic dipole moment along the

x-direction,  $m_z$  is the magnetic dipole moment along the z-direction.

$$\tan(\theta_{B,MD,s-pol}) = \frac{m_x}{m_z} \quad (8)$$

For p-polarized quadrupoles, we obtain a condition for each polarization.  $EQ_{xz}$  is the electric quadrupole moment in the x-z plane,  $EQ_{zz}$  is the electric quadrupole moment in the z direction and  $EQ_{xx}$  is the electric quadrupole moment in the x direction.  $MQ_{zy}$  is the magnetic quadrupole moment in the z-y plane and  $MQ_{xy}$  is the magnetic quadrupole moment in the x-y plane.

$$\tan(2\theta_{B,EQ,p-pol}) = -\frac{2EQ_{xz}}{EQ_{zz} - EQ_{xx}} \quad (9)$$

$$\tan(\theta_{B,MQ,p-pol}) = -\frac{MQ_{zy}}{MQ_{xy}} \quad (10)$$

For s-polarized quadrupoles, we obtain a condition for each polarization.  $EQ_{zy}$  is the electric quadrupole moment in the z-y plane.  $MQ_{xz}$  is the magnetic quadrupole moment in the x-z plane,  $MQ_{zz}$  is the magnetic quadrupole moment in the z direction and  $MQ_{xx}$  is the magnetic quadrupole moment in the x direction.

$$\tan(\theta_{B,EQ,s-pol}) = \frac{EQ_{zy}}{EQ_{xy}} \quad (11)$$

$$\tan(2\theta_{B,MQ,s-pol}) = -\frac{2MQ_{xz}}{MQ_{zz} - MQ_{xx}} \quad (12)$$

Unlike their dipole counterparts, the quadrupole Brewster angles can occur for both polarizations at different angles, suggesting that it may be possible to

engineer materials with both s- and p-polarized Brewster angles at different angles for the same wavelength. These new Brewster angles are shown schematically in Figure 1 (c) and (d), where two Brewster angles occur for each multipole.

To demonstrate equations 5 and 8-12, we study a 455 nm thick film of free-standing SiN, with a dispersive refractive index detailed in the supplemental information, section S5. The expected Brewster angle calculated from equation 1 is roughly 64 degrees corresponding to a refractive index of 2.0. We calculate the inverse tangent for equations 5 and 8-12 and show in Figure 2 where they intersect with the angle of incidence, which represents the Brewster angle condition in equation 7 being satisfied for each individual multipole. The y-axis plots the real part of the complex angle, while the scatter plot and colour scale indicate the imaginary part of the angle.

In Figure 2 (a), the p-polarized electric dipole angle is plotted, and it is shown that the real part of the angle intersects with the angle of incidence at the expected position of the Brewster angle at roughly 64 degrees. At the same time, the dark blue colour shows where the imaginary part is zero and which is now in addition to the Brewster angle condition in equation 5.

The p-polarized EQ and MQ angles are plotted in Figure 2 (b)-(c). For the p-polarized EQ Brewster angle in Figure 2 (b) this is roughly 45 degrees at a wavelength of 1800 nm. For the p-polarized MQ Brewster angle in Figure 2 (c) this is roughly at 42 degrees at a wavelength of 1700 nm.

For the s-polarized Brewster angles in Figure 2 (d)-(e), we observe that the MD and EQ Brewster angles occur at the same angle of roughly 64 degrees as

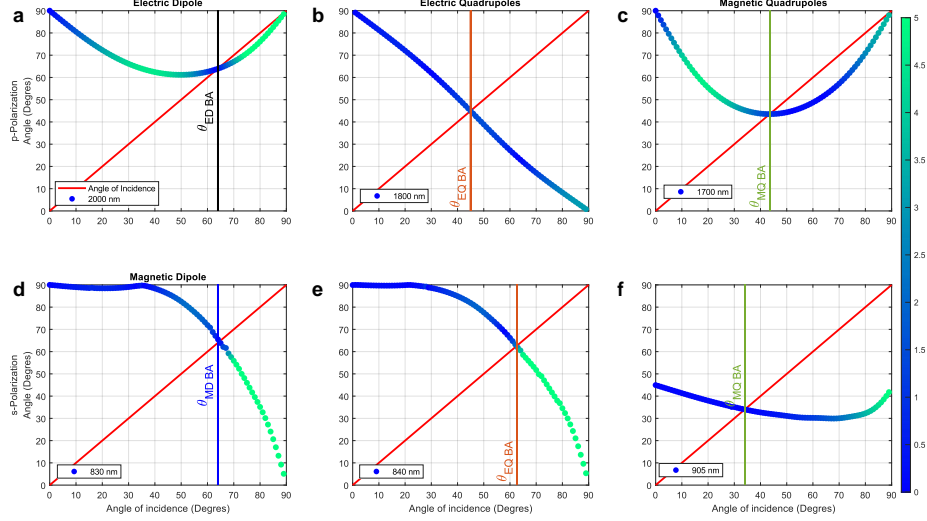


**Fig. 2** Demonstration of the Brewster angle condition,  $\theta_{ED,real} - \theta_I + i\theta_{ED,imag} = 0^\circ + 0i$  being satisfied for p-polarized reflected rays for the (a) electric dipole, (b) electric quadrupole, (c) magnetic quadrupole and s-polarized reflected rays, (d) magnetic dipole, (e) electric quadrupole, (f) magnetic quadrupole. The Brewster angle condition is satisfied when the real part of the angle of the multipole aligns with the angle of incidence, as marked by the intersection point with the red line, as well as the imaginary part of the angle of the multipole being zero, marked by the dark blue colour. The colour represents the imaginary angle. The imaginary angle can be related to the magnitude of the imaginary part of  $\vec{p}$  through the relation  $\theta_{ED,i} = \text{arcsinh}\left(\frac{|\text{imag}(\vec{p})|}{|\vec{p}|}\right)$ . Both conditions must be satisfied for a Brewster angle to occur in the multipole model.

the ED case (at 830 nm). We can now say that the well-known Brewster angle equation applies to p-polarized light for the ED case and s-polarized incident light for the MD and EQ cases as shown in equation 13.

It is possible to demonstrate that the magnetic dipole Brewster angle, equation 8, leads to the same tangent equation as the electric dipole Brewster angle in equation 5, as is shown in supplemental information section S1.3. Assuming the toroidal part of the EQ term is sufficiently small, then the behavior of the s-polarization EQ Brewster angle is the same as that of the MD, which we demonstrate in the supplemental material S2.6. A similar equivalence has been demonstrated in the reflection coefficients of these two multipoles for normal incidence

elsewhere [21]. The magnetic quadrupole Brewster angle occurs at 34 degrees and 905 nm, see Figure 2 (f).

$$\tan(\theta_B) = \frac{p_x}{p_z} = \frac{m_x}{m_z} = \frac{EQ_{zy}}{EQ_{xy}} = n \quad (13)$$

### 3 Experiment and simulation of reflection from a thin-film of silicon nitride

While we have derived new Brewster angles associated with each individual multipole, in order to describe the reflection of a thin film, we need to consider all multipoles together as described in equation 2, as equations 5, 8-12 only

identify the angles at which the Brewster angle occurs. It has been previously demonstrated that the reflection spectra, at normal incidence, of a thin film is composed of many multipoles interfering with each other [21].

We study how our model predicts the angle dependent reflection spectra of a SiN thin film. SiN is fast becoming the key material platform for much of integrated photonics from comb sources to single photon emitters [22]. We investigate through experiment and modeling a free-standing 455 nm thin film of SiN supported by a Si frame at a single wavelength of 1500 nm in Figure 3 and over a wavelength range from 750-2200 nm in Figure 4. The SiN sample is shown in

Figure 3 (a) and the experimental set up is shown in Figure 3 (b).

Figure 3 (c)-(d), verifies equation 2, which is our multipole model as a whole, where we describe the reflection of our SiN thin film in terms of the combined effects of the electric and magnetic multipoles. There is excellent agreement between the multipole and S-parameter models over the angles and wavelength studied.

In Figure 3 (c)-(d) we plot the magnitude of the individual reflection coefficients for the ED, MD, EQ and MQ terms for p- and s- polarized incident light as a function of angle of incidence. We neglect contributions from the octopoles terms in equation 2. Figure 3 (g)-(h) shows the

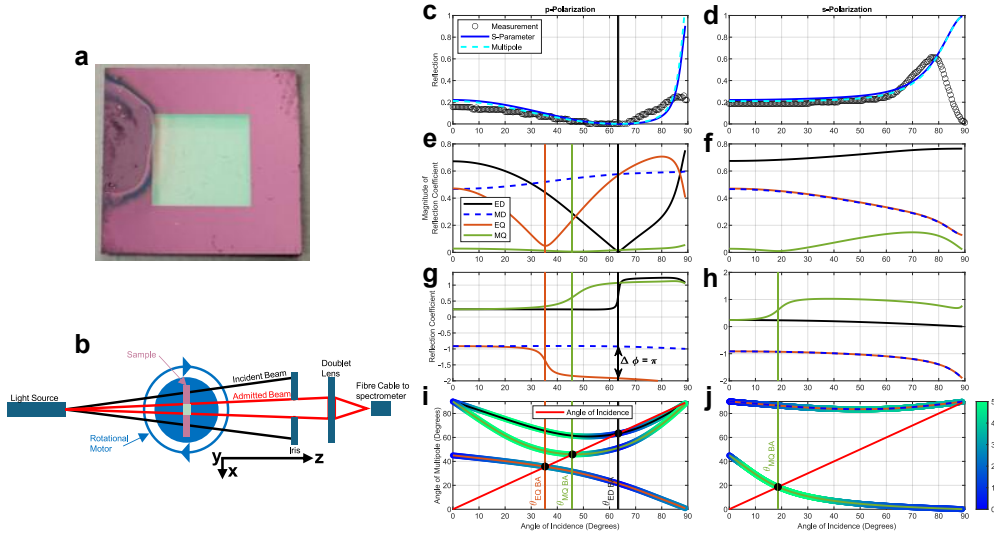


**Fig. 3** Comparison of our multipole model with the S-parameter simulation and experiment via a study of (a) free standing SiN thin film of thickness 455 nm at a wavelength of 1500 nm. (b) Schematic of experiment to measure reflection. (c)-(d) Comparison between measured (circles) and modelled reflection with S-parameter (blue line) and multipole decomposition (dashed cyan line) for both s-polarization (c) and p-polarization (d). (e)-(f) Amplitude of individual multipole reflection coefficients, ED (black line), MD (dashed blue line), EQ (orange line), MQ (green line) in the multipole model for both s-polarization (e) and p-polarization (f). (g)-(h) Phase of individual multipole reflection coefficients in the multipole model, phases are divided by  $\pi$ . (i)-(j) Angle of multipoles as previously shown in Figure 2 for both s-polarization (i) and p-polarization (j), Vertical black, green and orange lines mark the ED, MQ and EQ Brewster angles.

relative phase (with respect to the phase of the incident light) of the various multipoles while Figure 3 (i)-(j) shows the angle of the multipoles. From Figure 3 (i), we can identify the positions of the Brewster angles. At 64 degrees, the contribution of the ED term is indeed zero as expected,  $|r_{ED, p-pol}| = 0$ . We additionally note that at the Brewster angle, the phase of the electric dipole coefficient undergoes a  $\pi$  phase shift, and this serves as another way to identify the Brewster angle. We note the new result that the MD and EQ terms are large and equal but according to Figure 3 (g) are out of phase by  $\pi$  so that  $|r_{MD, p-pol}| + |r_{EQ, p-pol}| = 0$ , maintaining the well-known zero in reflection at this angle.

There is a MQ Brewster angle at 46 degrees and an EQ Brewster angle at 35 degrees. However, these are incomplete Brewster angles, as the reflection minima are not perfectly zero as seen in Figure 3 (e) and the imaginary angles are non-zero. These Brewster angles are wavelength specific, and the studied wavelength is close to the ideal wavelength to observe these Brewster angles, as seen in extend data figure, Figure 5 (d),(e),(f),(g) and (h). These however do not result in zero or near zero reflection due to incomplete cancellation of other multipoles (Figure 3 (c)). The same analysis is shown for s-polarized light in Figure 3 (d)-(j). Only a single MQ Brewster angle is found in this case at 19 degrees, but this is incomplete at this wavelength, due to the non-zero imaginary angle and due to incomplete cancellation from the other multipoles, a zero in reflection (Figure 3 (d)) is not found.

To fully explore the agreement between experiment and model, we plot the reflection spectra from 750-2200 nm and 0-70 degrees angle of incidence for

p- and s-polarized light. These maps are shown in Figure 4 and again show the excellent agreement between the multipole model and the S-parameter model and good agreement with the experimental data. We see the clear presence of the 1st and second Fabry Perot modes that will also result in zero reflection for both polarizations. The regions of zero reflection match perfectly with the expected location of the Fabry Perot modes, whose location is calculated with equation S.74 in the supplementary information and marked with the magenta lines.

By comparing experiment and theory, including the replication of the Brewster angle and Fabry Perot modes we conclude that our multipole model is a highly effective representation of the optical response of our thin film. The multipoles model in Figure 4 (b) and (g) begins to break down at larger angles and shorter wavelengths, given that higher order multipoles in the model are required as the film thickness approaches the wavelength of the incident light [21].

As highlighted earlier, the new Brewster angles are wavelength dependent, and this is shown clearly in Figures 4 (d), (e), (i) and (j). Here we plot the reflection coefficients for each multipole but over a very limited range from 0 to 0.1 so that Brewster angle positions can be clearly seen, unlike Figure 3 we required octupoles to accurately predict reflection at shorter wavelengths. In p-polarization, for the ED, we note the Brewster angle can be seen at all wavelengths near 64 degrees. The EQ BA occurs near 35 degrees in the wavelength range from 2200 nm down to 1400 nm. In s-polarization, we first note that the MD and EQ maps are identical as we met earlier. The Brewster angle occurs at 64 degrees in agreement with equation

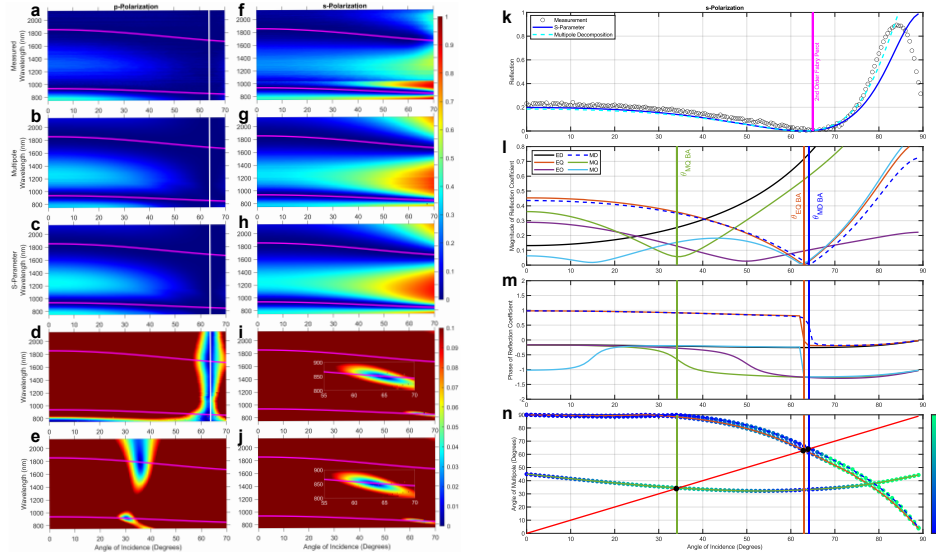


**Fig. 4** Broader comparison between simulations and experiment from wavelengths 750-2200 nm, (a) and (f) measured reflection, (b) and (g) multipole reflection, (c) and (h) S-parameter reflection for both s- and p-polarizations respectively, magenta lines represent the first 2 Fabry Perot modes plotted by equation S.74. (d)-(j) Individual reflection coefficients for electric dipole (d), magnetic dipole, (e) and (j) electric quadrupoles for p- and s-polarization over a limited range of reflection from 0 to 0.1 to identify the Brewster angles. (k)-(n) Investigation of SiN thin film at 850 nm, where the MD and EQ BAs are present similar to Figure 3. (k) Comparison between measured and modelled reflection. (l) Magnitude of individual reflection coefficients. (m) Phase of individual reflection coefficients. (n) Angle of MD, EQ and MQ multipoles.

13 (and Figure 5 (d)), but most striking is the very narrow range of wavelengths ( $\sim 30$  nm) over which it occurs in stark contrast to the ED case. If we examine the reflection from both experiment and simulations at 850 nm for s-polarized as a function of angle, we plot the results in Figure 4, (k), (l), (m), (n). We note in Figure 4 (k), the reflection is zero around 64 degrees but that this position also coincides with a Fabry Perot resonance, which happens to intersect with these Brewster angles. As discussed in supplemental material S4, Fabry Perot modes and Brewster angles are distinctly different interference phenomena which happen to overlap at this wavelength and angle. In Figure 4, (l), we see the MD and EQ Brewster angles but we

note also the ED, MQ and EO terms are non-zero but their interference produces the zero in reflection. The magnetic quadrupole is an incomplete Brewster angle, given the reflection minima and imaginary angle are non-zero. There appears to be evidence of octupole Brewster angles in Figure 4 (l), the magnetic octupole, which shows two minima at 15 and 64 degrees respectively and the electric octupole, which shows a single minima at 40 degrees.

## 4 Outlook

We have demonstrated a fundamental analysis of the p-polarized Brewster angle, showing how it arises from the electric dipole response of a medium,

with verification in an experiment with a free-standing SiN thin film. Our analysis reveals a previously hidden feature of this Brewster angle, the destructive interference of electric and magnetic multipoles is also essential to obtaining a zero reflection minimum. This work also highlights how other multipoles, including the magnetic dipole quadrupoles and octupoles may also satisfy the well-known Brewster angle condition. These new Brewster angles can support both s- and p-polarized Brewster angles at the same wavelength, a feature not possible in dipole Brewster angles.

However, they are hidden in the reflection spectra of thin films, as the destructive interference between remaining multipoles is incomplete. This provides a possible opportunity for metamaterials to realize these new Brewster angle, as our model and equations are directly applicable to metamaterials, when the substrate and superstrate have the same refractive index.

The origin of the magnetic response at these optical frequencies where the permeability,  $\mu$ , is 1 has been a subject of very active research [9, 20, 21, 23, 24]. Clearly, there is a strong high frequency magnetic response in our materials as is made clear through the multipole model. Landau and Lifshitz [25] developed the argument that spatial dispersion of the refractive index results in a magnetic response and this argument has been expanded on by the work of Agranovich [26]. Our thin film SiN sample featuring zero reflection with Fabry Perot and Brewster angle effects is exhibiting such spatial dispersion. Like the work of [21], a magnetic response is demonstrated without the need for metamaterials.

The pseudo-Brewster angle which shows a non-zero reflection minimum

in p-polarization for lossy materials can also be accounted for with our model. The non-zero reflection has been demonstrated to occur due to be a lack of alignment of the electric dipole with angle of incidence, as well as an angular shift in the destructive interference between magnetic dipole and electric quadrupole (see supplementary materials, section 7).

## 5 Methods

**Multipole Decomposition** Equation 2 [27] in the main text was used to model the complex reflection coefficients, the individual terms are outlined below.  $\omega$  is the frequency,  $k_d$  is the wavenumber in the surrounding dielectric,  $\epsilon_d$  is the permittivity of the surrounding dielectric,  $\epsilon_0$  is the permittivity of free space,  $E_0$  is the incident electric field and  $S_L$  is the surface area of the unit cell. This unit cell is defined as a cube with dimensions equal to the thickness of our thin film. In equation 2 the first term in the square brackets is the electric dipole with  $\vec{p}$  the electric dipole moment and  $\vec{n}$  is the direction of reflection. These are related to the angle of incidence and wavevector of the incident light as shown in Figure 1 (a). The second term is the magnetic dipole moment,  $\vec{m}$ , Figure 1 (b). The third term is the electric quadrupole moment,  $\hat{Q}$ , Figure 1 (c). The fourth term is the magnetic quadrupole moment,  $\hat{M}$ , Figure 1 (d). The fifth and sixth terms,  $\hat{O}^e$  is the electric octupole moment and  $\hat{O}^m$  is the magnetic octupole moment. These multipole moments are calculated with volume integrals, where we integrate the electric field over the volume of a unit cell of the thin film.

$$\phi = \tan \left( \frac{r_{multipole,r}}{r_{multipole,i}} \right)$$

$\phi$  is the phase of the reflection coefficient, which gives us useful information on how the phase response of the incident electric field is shifted by each multipole, which is important when understanding the constructive ( $0, 2\pi, 4\pi,$ etc) and destructive ( $1\pi, 3\pi, 5\pi,$ etc) interference that occurs in thin films in terms of multipoles.

The reflection coefficients for the electric dipole,  $\vec{n} \times (\vec{p} \times \vec{n})$ , is as follows. The first row is sufficient for p-polarized light, while the second row is sufficient for s-polarized light.

$$\begin{pmatrix} \cos(\theta_I)(p_x \cos(\theta_I) - p_z \sin(\theta_I)) \\ p_y \\ \sin(\theta_I)(p_z \sin(\theta_I) - p_x \cos(\theta_I)) \end{pmatrix} \quad (14)$$

And for the magnetic dipole,  $\vec{m} \times \vec{n}$ .

$$\begin{pmatrix} -m_y \cos(\theta_I) \\ -m_z \sin(\theta_I) + m_x \cos(\theta_I) \\ m_y \sin(\theta_I) \end{pmatrix} \quad (15)$$

For the electric quadrupole,  $\vec{n} \times (\vec{n} \times (\hat{E}Q\vec{n}))$

$$\begin{pmatrix} \cos^2(\theta_I) \sin(\theta_I)(EQ_{xx} - EQ_{yy}) + \cos(\theta_I)(EQ_{xz} \cos^2(\theta_I) - EQ_{zx} \sin^2(\theta_I)) \\ EQ_{yx} \sin(\theta_I) + EQ_{xz} \cos(\theta_I) \\ \cos(\theta_I) \sin^2(\theta_I)(EQ_{zy} - EQ_{xx}) + \sin(\theta_I)(EQ_{zx} \sin^2(\theta_I) - EQ_{xz} \cos^2(\theta_I)) \end{pmatrix}$$

For the magnetic quadrupole,  $\vec{n} \times (\hat{M}Q\vec{n})$ .

$$\begin{pmatrix} -\cos(\theta_I)(MQ_{yx} \sin(\theta_I) + MQ_{yz} \cos(\theta_I)) \\ \cos(\theta_I) \sin(\theta_I)(MQ_{xx} - MQ_{zz} + MQ_{xz} \cos^2(\theta_I) - MQ_{zx} \sin^2(\theta_I)) \\ \sin(\theta_I)(MQ_{yx} \sin(\theta_I) + MQ_{xz} \cos(\theta_I)) \end{pmatrix}$$

For the electric octupole,  $\vec{n} \times (\vec{n} \times \hat{O}(\vec{n}\vec{n}))$ .

$$\begin{pmatrix} \cos(\theta_I)[O_{zzz} \cos^3(\theta_I) - O_{xzx} \sin^3(\theta_I) + \cos^2(\theta_I) \sin(\theta_I)(2O_{zxx} - O_{zzz}) \\ + \cos(\theta_I) \sin^2(\theta_I)(O_{zxx} - 2O_{zzx})] \\ O_{zyz}[\cos^2(\theta_I) \sin^2(\theta_I)] + 2O_{zyx}[\sin^3(\theta_I) \cos(\theta_I) - \cos^3(\theta_I) \sin(\theta_I)] \\ + O_{xyy}[\sin^4(\theta_I) - \cos^2(\theta_I) \sin^2(\theta_I)] \\ - \sin(\theta_I)[O_{zzz} \cos^3(\theta_I) - O_{xzx} \sin^3(\theta_I) + \cos^2(\theta_I) \sin(\theta_I)(2O_{zxx} - O_{zzz}) \\ + \cos(\theta_I) \sin^2(\theta_I)(O_{zxx} - 2O_{zzx})] \end{pmatrix} \quad (16)$$

For the magnetic octupole,  $\vec{n} \times \hat{O}(\vec{n}\vec{n})$ .

$$\begin{pmatrix} -O_{zyz} \cos^3(\theta_I) - 2O_{zyx} \cos^2(\theta_I) \sin(\theta_I) - O_{xyx} \cos(\theta_I) \sin^2(\theta_I) \\ O_{zzz} \cos^3(\theta_I) - O_{xzx} \sin^3(\theta_I) + \cos^2(\theta_I) \sin(\theta_I)(2O_{zxx} - O_{zzz}) \\ + \cos(\theta_I) \sin^2(\theta_I)(O_{zxx} - 2O_{zzx}) \\ O_{zyz} \cos^2(\theta_I) \sin(\theta_I) + 2O_{zyx} \cos^2(\theta_I) \sin(\theta_I) + O_{xyx} \sin^3(\theta_I) \end{pmatrix} \quad (17)$$

The multipole moments are calculated in COMSOL using a 3D simulation, using Floquet periodic boundary conditions to define an infinitely wide film, the physical dimensions of the film in the simulation volume was a cube with dimensions equal to the film thickness, 455 nm. The multipole moments presented in equations 13-16 are calculated using volume integrals with the following equations, where  $a$  and  $b$  defines the cartesian axes that current densities are integrated over.

$$\vec{p}_a = \frac{i}{\omega} \int_V j_0(k_d r) J_a dV + \int_V \frac{ik_d^2}{\omega^2} (\vec{r} \cdot \vec{J}) \cdot \vec{r} - \vec{r}^2 \cdot \vec{J} dV \quad (18)$$

$\vec{J} = -i\omega(\epsilon_{SiN} - \epsilon_{air})\vec{E}$  is the current density.  $j_0$  is the bessel function of the first kind. The magnetic dipole moment,  $\vec{m}_a$ , along cartesian co-ordinate  $a$ , is described as follows.

$$\vec{m}_a = \frac{3ik_d}{2} \int_V \frac{j_1(k_d r)}{k_d r} (\vec{r} \times \vec{J})_a dV \quad (19)$$

The magnetic dipole moment, and all following multipoles have an origin dependence, and the moments of these multipoles appear to depend on selection of a reference point, we set our origin to the  $x, y, z$  co-ordinates  $0, 0, 0$  and ensure that the center of our thin film/unit cell is located at this origin.

The electric quadrupole moment, which includes a second, toroidal term is:

$$\begin{aligned} \hat{Q}_{ab} = & \frac{-ik_d}{2} \int_V \frac{j_1(k_d r)}{k_d r} (3(\vec{r}_a \vec{J}_b - \vec{J}_a \vec{r}_b) - 2(\vec{r}_a \cdot \vec{J}_b) \hat{U}_{ab}) dr \\ & + \frac{6ik_d^2}{\omega} \int_V \frac{j_3(k_d r)}{k_d^3 r^3} [5(\vec{J} \cdot \vec{r}) \vec{r}_a \vec{r}_b - r^2 (\vec{J}_a \vec{r}_b + \vec{r}_a \vec{J}_b) - (\vec{J} \cdot \vec{r}) r^2 \hat{U}] dr \end{aligned} \quad (20)$$

The magnetic quadrupole moment is:

$$\hat{M}_{ab} = \frac{5k_d^2}{2} \int_V \frac{j_2(k_d r)}{(k_d r)^2} ([\vec{r} \times \vec{J}]_a \vec{r}_b + \vec{r}_a [\vec{r} \times \vec{J}]_b) dr \quad (21)$$

The electric octupole moment is:

$$O_{abc}^{\hat{e}} = \frac{15k_d^2}{\omega} \int_V \frac{j_2(k_d r)}{(k_d r)^2} (\vec{J}_a \vec{r}_b \vec{r}_c + \vec{r}_a \vec{J}_b \vec{r}_c + \vec{r}_a \vec{r}_b \vec{J}_c - \hat{A}) dr \quad (22)$$

The magnetic octupole moment is:

$$\begin{aligned} O_{abc}^{\hat{m}} = & \frac{105}{4} \int_V \frac{j_3(k_d r)}{(k_d r)^3} ([\vec{r} \times \vec{J}]_a \vec{r}_b \vec{r}_c + \vec{r}_a [\vec{r} \times \vec{J}]_b \vec{r}_c + \\ & \vec{r}_a [\vec{r} \times \vec{J}]_b \vec{r}_c + \vec{r}_a \vec{r}_b [\vec{r} \times \vec{J}]_c - \hat{A}'_{abc}) dr \end{aligned} \quad (23)$$

**Sample Characterization** Samples were purchased from Silson [28]. To measure light transmission through our SiN sample, we constructed a home-built set up automated with MATLAB. A detailed guide on calibration methodology is presented in the supplemental material S8, as well as details of exact components used. To measure transmission across wavelengths from 750-2200 nm we used a tungsten halogen lamp, which was connected to a fiber cable, and terminated with a free space collimator. Polarization of incident light was controlled with a Glan-Thompson polarizer, the sample was held with clamps on the Si frame supporting the free-hanging SiN, which was joined to a rotational motor to change the angle of incidence. An iris was placed after the sample to reduce the possible range of angle of incidence resulting from a diverging beam. Finally, a lens was used to focus the light into a fiber cable joined to either the visible (400-1000 nm) or near-infrared spectrometers (1000-2200 nm). The reflection spectra presented in the paper were calculated with  $R=1-T$  with absorption set to zero.

The thickness and refractive indices of this film were measured by ellipsometry and presented in supplementary information section S5.6. Our refractive indices were only measured between 200-900 nm, and we extrapolated our fitted equations to 2200 nm assuming that the imaginary part of the refractive index was zero.

**Acknowledgments.** This work was supported under the AMBER research centre platform funding from Research Ireland under grant number 12/RC/2278P2.



## 6 Extended Data Figures

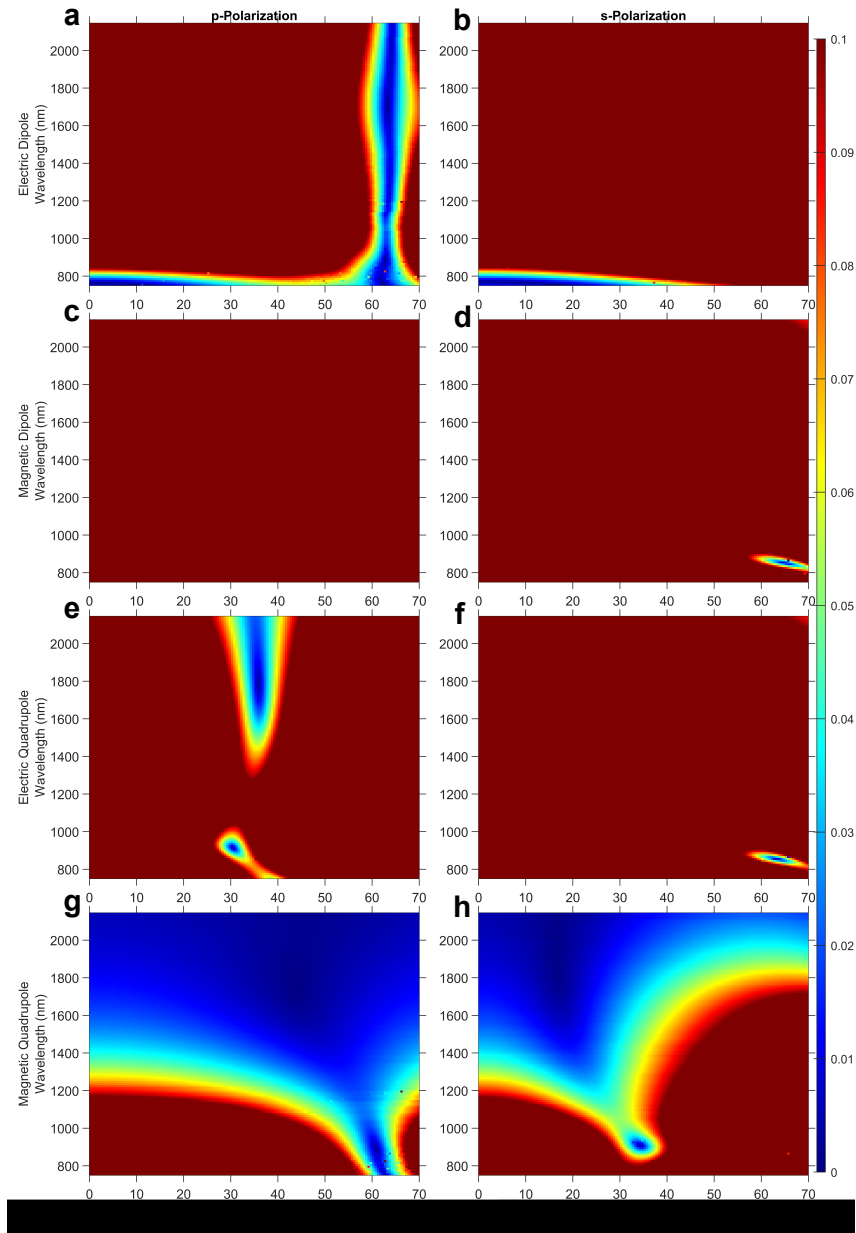


**Fig. 5** Magnitude of reflection coefficients for individual multipoles for p- and s-polarization. Colour map is restricted to reflection in the range 0-0.1 to highlight reflection minima corresponding to the multipole. (a) p-polarized ED, (b) s-polarized ED. (c) p-polarized MD and (d) s-polarized MD. (e) p-polarized EQ and (f) s-polarized EQ. (g) p-polarized MQ and (h) s-polarized MQ.

## References

- [1] Brewster, D.: X. On the laws which regulate the polarisation of light by reflexion from transparent bodies. By David Brewster, LL. D. F. R. S. Edin. and F. S. A. Edin. In a letter addressed to Right Hon. Sir Joseph Banks, Bart. K. B. P. R. S.. *Philosophical Transactions of the Royal Society of London* **105**, 125–159 (1815) <https://doi.org/10.1098/rstl.1815.0010>
- [2] Lakhtakia, A.: Would Brewster recognize today’s Brewster angle? *Optics News* **15**(6), 14–18 (1989) <https://doi.org/10.1364/ON.15.6.000014>
- [3] Sreekanth, K.V., ElKabbash, M., Medwal, R., Zhang, J., Letsou, T., Strangi, G., Hinczewski, M., Rawat, R.S., Guo, C., Singh, R.: generalized Brewster Angle Effect in Thin-Film Optical Absorbers and Its Application for Graphene Hydrogen Sensing. *ACS Photonics* **6**(7), 1610–1617 (2019) <https://doi.org/10.1021/acsp Photonics.9b00564> .
- [4] Paniagua-Domínguez, R., Yu, Y.F., Miroschnichenko, A.E., Krivitsky, L.A., Fu, Y.H., Valuckas, V., Gonzaga, L., Toh, Y.T., Kay, A.Y.S., Lukyanchuk, B., Kuznetsov, A.I. Generalized Brewster effect in dielectric metasurfaces. *Nat Commun* **7** (2016) <https://doi.org/10.1038/ncomms10362>
- [5] Zhang, Z., Che, Z., Liang, X., Chu, J., Zeng, J., Huang, H., Guan, F., Shi, L., Liu, X., Zi, J.: Realizing Generalized Brewster Effect by Generalized Kerker Effect.. *Phys. Rev. Appl.* **16**, 054017 (2021) <https://doi.org/10.1103/PhysRevApplied.16.054017>
- [6] Tiukuvaara, V., Martin, O.J.F., Achouri, K.: Quadrupolar susceptibility modeling of substrated metasurfaces with application to the generalized Brewster effect. *Opt. Express* **31**(14), 22982–22996 (2023) <https://doi.org/10.1364/OE.488529>
- [7] Evlyukhin, A.B., Novikov, S.M., Zywietz, U., Eriksen, R.L., Reinhardt, C., Bozhevolnyi, S.I., Chichkov, B.N.: Demonstration of Magnetic Dipole Resonances of Dielectric Nanospheres in the Visible Region. *Nano Lett* **12** (2012) <https://doi.org/10.1021/nl301594s>
- [8] Majorel, C., Patoux, A., Estrada-Real, A., Urbaszek, B., Girard, C., Arbouet, A., Wiecha, P.R.: Generalizing the exact multipole expansion: Density of multipole modes in complex photonic nanostructures. *Nanophotonics* **11**, 3663–3678 (2022) <https://doi.org/10.1515/nanoph-2022-0308>
- [9] Monticone, F., Alù, A.: The quest for optical magnetism: From split-ring resonators to plasmonic nanoparticles and nanoclusters. *Journal of Materials Chemistry C* **2** (2014) <https://doi.org/10.1039/c4tc01406e>
- [10] Kaelberer, T., Fedotov, V.A., Papasimakis, N., Tsai, D.P., Zheludev, N.I.: Toroidal Dipolar Response in a Metamaterial. *Science* **330**, 1510–2 (2010) <https://doi.org/10.1126/science.1192711>

[//doi.org/10.1126/science.1197172](https://doi.org/10.1126/science.1197172)

- [11] Savinov, V., Papasimakis, N., Tsai, D.P., Zheludev, N.: Optical anapoles. *Commun Phys* **2**, 69 (2019) <https://doi.org/10.1038/s42005-019-0167-z>
- [12] Baryshnikova, K.V., Smirnova, D.A., Luk'yanchuk, B.S., Kivshar, Y.S.: Optical anapoles: Concepts and applications. *Advanced Optical Materials* **7** (2019) <https://doi.org/10.1002/adom.201801350>
- [13] Miroschnichenko, A.E., Evlyukhin, A.B., Yu, Y.F., Bakker, R.M., Chipouline, A., Kuznetsov, A.I., Luk'yanchuk, B., Chichkov, B.N., Kivshar, Y.S.: Nonradiating anapole modes in dielectric nanoparticles. *Nature Communications* **6** (2015) <https://doi.org/10.1038/ncomms9069>
- [14] Terekhov, P.D., Babicheva, V.E., Baryshnikova, K.V., Shalin, A.S., Karabchevsky, A., Evlyukhin, A.B.: Multipole analysis of dielectric metasurfaces composed of nonspherical nanoparticles and lattice invisibility effect. *Physical Review B* **99** (2019) <https://doi.org/10.1103/PhysRevB.99.045424>
- [15] Alaei, R., Safari, A., Sandoghdar, V., Boyd, R.W.: Kerker effect, superscattering, and scattering dark states in atomic antennas. *Phys. Rev. Res.* **2**, 043409 (2020) <https://doi.org/10.1103/PhysRevResearch.2.043409>
- [16] Bukharin, M., Pecherkin, V., Ospanova, A., Il'in, V., Vasilyak, L., Basharin, A., Lukiyanichuk, B. Transverse kerker effect in all-dielectric spheroidal particles *Sci Rep*,12, 7997 (2022) <https://doi.org/10.21203/rs.3.rs-947900/v1>
- [17] Merlin, R. Metamaterials and the landau-Lifshitz permeability argument: Large permittivity begets high-frequency magnetism. *Proceedings of the National Academy of Sciences of the United States of America* **106** (2009) <https://doi.org/10.1073/pnas.0808478106>
- [18] Shafiei, F., Monticone, F., Le, K.Q., Liu, X.X., Hartsfield, T., Alù, A., Li, X. A subwavelength plasmonic metamolecule exhibiting magnetic- based optical fano resonance. *Nature Nanotechnology* **8** (2013) <https://doi.org/10.1038/nnano.2012.249>
- [19] Pendry, J.B.: Negative refraction. *Contemporary Physics* **45**(3), 191–202 (2004) <https://doi.org/10.1080/00107510410001667434>
- [20] Papadakis, G.T., Fleischman, D., Davoyan, A., Yeh, P., Atwater, H.A. Optical magnetism in planar metamaterial heterostructures. *Nature Communications* **9** (2018) <https://doi.org/10.1038/s41467-017-02589-8>
- [21] Li, J., Papasimakis, N., MacDonald, K.F., Zheludev, N.I. Optical magnetic response without metamaterials. *APL Photonics* **6** (2021) <https://doi.org/10.1063/5.0054752>

- [22] Enjavi, Mohammad, Javadizadeh, Saeed Adibi, Ali .Silicon Nitride: From Workhorse to Superstar Optics and Photonics News **36. 42** (2025) <https://doi.org/10.1364/OPN.36.11.000042>
- [23] Man, M., Webb, K.J.: On the Microscopic Origins of Optical Magnetism — Insight from Mie Theory. *Frontiers in Optics 2016, OSA Technical Digest* (2016). <https://doi.org/10.1364/FIO.2016.JW4A.5>
- [24] Monticone, F., Alu, A. Metamaterial, plasmonic and nanophotonic devices. *Reports on Progress in Physics* **80** (2017) <https://doi.org/10.1088/1361-6633/aa518f>
- [25] Landau, L.D., Lifshitz, E.M., Chapter XII - Spatial Dispersion, In *Course of Theoretical Physics, Electrodynamics of continuous media*. (Second Edition) **29** (1984) <https://doi.org/10.1016/B978-0-08-030275-1.50018-7>
- [26] Agranovich, V.M., Gartsstein, Y.N. Spatial dispersion and negative refraction of light. *Uspekhi Fizicheskikh Nauk* **176** (2006) <https://doi.org/10.3367/ufnr.0176.200610c.1051>
- [27] Evlyukhin, A.B., Chichkov, B.N. Multipole decompositions for directional light scattering. *Physical Review B* **100** (2019) <https://doi.org/10.1103/PhysRevB.100.125415>
- [28] Silicon nitride membranes - dielectric substrate materials. <https://silson.com/product/silicon-nitride-membranes/>. Accessed: 2024-01-27

Supplementary information.

## 1 Deriving Angle Dependence in Multipole Decomposition

This section outlines our modification to the multipole model discussed in the previous section, to expand it to all angles of incidence.

To extend to all angles of incidence, we make the scattering direction,  $\vec{n}$ , varying as a function of the angle of incidence, as seen below in equation S.1 and perform a series of inner tensor products and cross products to derive the angle dependence contribution to the reflected field from each multipole. When investigating the reflected field, the scattering angle,  $\theta_I$  will be rotated by -180 degrees relative to the angle of incidence. The relation between the scattering angle in the reflection direction, and the angle of incidence,  $\theta_I$ , is as follows,  $\theta_{scattering} = \theta_I - 180^\circ$ . The direction of scattering/angle of incidence can be defined as a unit vector that would be associated with the wavevector of the light and is defined below.

$$\vec{n} = \begin{bmatrix} \sin(\theta_{scattering}) \\ 0 \\ \cos(\theta_{scattering}) \end{bmatrix} = \begin{bmatrix} -\sin(\theta_I) \\ 0 \\ -\cos(\theta_I) \end{bmatrix} \quad (\text{S.1})$$

To calculate the angle dependence for the dipoles, we perform a cross product between the dipole moment vector,  $\vec{a}$ , and the unit vector  $\vec{n}$ .

$$\vec{a} \times \vec{n} = \begin{bmatrix} -a_y \cos(\theta_I) \\ -a_z \sin(\theta_I) + a_x \cos(\theta_I) \\ a_y \sin(\theta_I) \end{bmatrix} \quad (\text{S.2})$$

Equation S.2 is sufficient for the magnetic dipole. To obtain the equations for the electric dipole contribution, we must perform another cross product.

$$\vec{n} \times (\vec{a} \times \vec{n}) = \begin{bmatrix} \cos(\theta_I)(a_x \cos(\theta_I) - a_z \sin(\theta_I)) \\ a_y \\ \sin(\theta_I)(a_z \sin(\theta_I) - a_x \cos(\theta_I)) \end{bmatrix} \quad (\text{S.3})$$

The vectors described in equations S.2 and S.3 describe the scattered field from the magnetic and electric dipoles for unpolarized light. For s-polarized light we only need the middle element in each vector, for p-polarized light we can use either the 1st or 3rd elements, or both, the other elements being zero. For simplicity, we only use the 1st element, as it is the only one valid at normal incidence.

To derive the contribution for the quadrupoles, we perform a tensor inner product between the quadrupole tensor  $\hat{A}$  and the unit vector  $\vec{n}$ , giving us a vector to perform cross products on.

$$\hat{A}\vec{n} = \begin{pmatrix} A_{xx} & A_{xy} & A_{xz} \\ A_{yx} & A_{yy} & A_{yz} \\ A_{zx} & A_{zy} & A_{zz} \end{pmatrix} \begin{pmatrix} -\sin(\theta_I) \\ 0 \\ -\cos(\theta_I) \end{pmatrix} = - \begin{pmatrix} A_{xx} \\ A_{yx} \\ A_{zx} \end{pmatrix} \sin(\theta_I) - \begin{pmatrix} A_{xz} \\ A_{yz} \\ A_{zz} \end{pmatrix} \cos(\theta_I) \quad (\text{S.4})$$

$$\hat{A}\vec{n} = \begin{pmatrix} -A_{xx}\sin(\theta_I) - A_{xz}\cos(\theta_I) \\ -A_{yx}\sin(\theta_I) - A_{zx}\cos(\theta_I) \\ -A_{zx}\sin(\theta_I) - A_{zz}\cos(\theta_I) \end{pmatrix} \quad (\text{S.5})$$

To obtain the magnetic quadrupole terms, a cross product between the above and the unit vector is performed.

$$\vec{n} \times (\hat{A}\vec{n}) = \begin{pmatrix} -\sin(\theta_I) \\ 0 \\ -\cos(\theta_I) \end{pmatrix} \times \begin{pmatrix} -A_{xx}\sin(\theta_I) - A_{xz}\cos(\theta_I) \\ -A_{yx}\sin(\theta_I) - A_{zx}\cos(\theta_I) \\ -A_{zx}\sin(\theta_I) - A_{zz}\cos(\theta_I) \end{pmatrix} \quad (\text{S.6})$$

$$\vec{n} \times (\hat{A}\vec{n}) = \begin{pmatrix} -\cos(\theta_I)(A_{yx}\sin(\theta_I) + A_{yz}\cos(\theta_I)) \\ \cos(\theta_I)\sin(\theta_I)(A_{xx} - A_{zz} + A_{zx}\cos^2(\theta_I) - A_{zx}\sin^2(\theta_I)) \\ \sin(\theta_I)(A_{yz}\sin(\theta_I) + A_{yz}\cos(\theta_I)) \end{pmatrix} \quad (\text{S.7})$$

Another cross product obtains the electric quadrupole contribution.

$$\vec{n} \times (\vec{n} \times (\hat{A}\vec{n})) = \begin{pmatrix} \cos^2(\theta_I)\sin(\theta_I)(A_{xx} - A_{yz}) + \cos(\theta_I)(A_{xz}\cos^2(\theta_I) - A_{zx}\sin^2(\theta_I)) \\ A_{yx}\sin(\theta_I) + A_{xz}\cos(\theta_I) \\ \cos(\theta_I)\sin^2(\theta_I)(A_{zx} - A_{xx}) + \sin(\theta_I)(A_{zx}\sin^2(\theta_I) - A_{xz}\cos^2(\theta_I)) \end{pmatrix} \quad (\text{S.8})$$

As with the dipoles, the 1st element is for p-polarized light, and the 2nd element is for s-polarized light.

The derivation follows the same steps as outlined for the octupole with an additional tensor product to reduce the order of the 3rd order octuple tensor, to a 1st order tensor required to perform cross products.

$$\hat{O}(\vec{n}\vec{n}) = \begin{pmatrix} -\sin(\theta_I)^2 O_{xxx} - 2\sin(\theta_I)\cos(\theta_I)O_{zxx} - \cos(\theta_I)^2 O_{zzz} \\ -\sin(\theta_I)^2 O_{xyx} - 2\sin(\theta_I)\cos(\theta_I)O_{zyx} - \cos(\theta_I)^2 O_{zyz} \\ -\sin(\theta_I)^2 O_{xzx} - 2\sin(\theta_I)\cos(\theta_I)O_{zzx} - \cos(\theta_I)^2 O_{zzz} \end{pmatrix} \quad (\text{S.9})$$

The magnetic octupole becomes the following.

$$\vec{n} \times \hat{O}(\vec{n}\vec{n}) = \begin{pmatrix} -O_{zyz}\cos^3(\theta_I) - 2O_{zyx}\cos^2(\theta_I)\sin(\theta_I) - O_{xyx}\cos(\theta_I)\sin^2(\theta_I) \\ O_{zxx}\cos^3(\theta_I) - O_{xzx}\sin^3(\theta_I) + \cos^2(\theta_I)\sin(\theta_I)(2O_{zxx} - O_{zzz}) \\ + \cos(\theta_I)\sin^2(\theta_I)(O_{zxx} - 2O_{zzx}) \\ O_{zyz}\cos^2(\theta_I)\sin(\theta_I) + 2O_{zyx}\cos^2(\theta_I)\sin(\theta_I) + O_{xyx}\sin^3(\theta_I) \end{pmatrix} \quad (\text{S.10})$$

And to obtain the electric octupole we perform a final cross product.

$$\vec{n} \times (\vec{n} \times \hat{O}(\vec{n}\vec{n})) =$$

$$\left( \begin{array}{c} \cos(\theta_I)[O_{zzz} \cos^3(\theta_I) - O_{zzx} \sin^3(\theta_I) + \cos^2(\theta_I) \sin(\theta_I)(2O_{zxx} - O_{zzz}) \\ \quad + \cos(\theta_I) \sin^2(O_{zxx} - 2O_{zzx})] \\ \\ O_{zyz}[\cos^2(\theta_I) \sin^2(\theta_I)] + 2O_{zyx}[\sin^3(\theta_I) \cos(\theta_I) - \cos^3(\theta_I) \sin(\theta_I)] \\ \quad + O_{xyy}[\sin^4(\theta_I) - \cos^2(\theta_I) \sin^2(\theta_I)] \\ \\ - \sin(\theta_I)[O_{zzz} \cos^3(\theta_I) - O_{zzx} \sin^3(\theta_I) + \cos^2(\theta_I) \sin(\theta_I)(2O_{zxx} - O_{zzz}) \\ \quad + \cos(\theta_I) \sin^2(O_{zxx} - 2O_{zzx})] \end{array} \right) \quad (\text{S.11})$$

To predict the reflection coefficients from these multipoles we use the equation below, using the cross product terms derived earlier to calculate the reflection coefficient in terms of these multipoles [1].

$$r_{s-pol} = \frac{ik_d}{E_0 2S_L \epsilon_0 \epsilon_d} (p_y + \frac{1}{v_d} m_y + \frac{ik_d}{6} Q_y + \frac{ik_d}{2v_d} M_y + \frac{k_d^2}{6} O_y^e + \frac{ik_d^2}{6v_d} O_y^m) \quad (\text{S.12})$$

$$r_{p-pol} = \frac{ik_d}{E_0 2S_L \epsilon_0 \epsilon_d} (p_x + \frac{1}{v_d} m_x + \frac{ik_d}{6} Q_x + \frac{ik_d}{2v_d} O_x^e + \frac{k_d^2}{6} O_x^m) \quad (\text{S.13})$$

$E_0$  is the incident electric field, which is taken at the origin of the simulation, in the absence of the thin film.  $S_L$  is the surface area exposed to the incident light,  $S_L = xy \cos(\theta_I)$ , the cosine function accounts for the changing surface area as the angle of incidence increase.  $\epsilon_d$  is the electric permittivity of the surrounding dielectric and  $v_d$  is the speed of light in the surrounding dielectric.

$p_a$  and  $m_a$  are the electric and magnetic dipole moments along the a-axis, where a = x, y, z.

$$p_a = (\vec{n} \times (\vec{a} \times \vec{n}))_a \quad (\text{S.14}) \quad m_a = (\vec{a} \times \vec{n})_a \quad (\text{S.15})$$

where  $Q_a$  and  $M_a$  are the electric and magnetic quadrupole moments.

$$Q_a = (\vec{n} \times (\vec{n} \times (\hat{M}\vec{n})))_a \quad (\text{S.16}) \quad M_a = (\vec{n} \times (\hat{M}\vec{n}))_a \quad (\text{S.17})$$

where  $O_a^e$  and  $O_a^m$  are the electric and magnetic octupole moments.

$$O_a^e = (\vec{n} \times (\vec{n} \times \hat{O}(\vec{n}\vec{n})))_a \quad (\text{S.18}) \quad O_a^m = (\vec{n} \times \hat{O}(\vec{n}\vec{n}))_a \quad (\text{S.19})$$

To characterize thin films that extend to infinity in the plane, we follow the same procedure applied to metamaterials, we define a single unit cell of the infinitely wide thin film, in this case that is a cube with dimensions equivalent to the thickness of the film, this matches previous models used to characterize thin films with multipole decomposition. We compute the scattered field associated with the multipole moments by integrating the current density,  $\vec{J}$ , as described in the main text, over the volume of this cube. Reflection is calculated by dividing this scattered field by the incident field at the centre of an empty unit cell.

## 2 Deriving Higher Order Brewster Angle Equations

This section outlines the derivation of the ED and new MD, EQ and MQ Brewster angles presented in the main text.

## 2.1 Electric Dipole Brewster Angle

To derive the electric dipole Brewster angle, we begin with the vector describing the reflected light from the electric dipole.

$$\vec{n} \times (\vec{p} \times \vec{n}) = \begin{bmatrix} r_{p-pol} \\ r_{s-pol} \\ r_{p-pol} \end{bmatrix} = \begin{bmatrix} \cos(\theta_I)(p_x \cos(\theta_I) - p_z \sin(\theta_I)) \\ p_y \\ \sin(\theta_I)(p_z \sin(\theta_I) - p_x \cos(\theta_I)) \end{bmatrix} \quad (\text{S.20})$$

For p-polarized light, we can consider the first or third elements of the vector, however the 3rd element is undefined at normal incidence, and can be ignored. The second element is related to s-polarized light, and has no angular dependence, hence no Brewster angle can be derived for s-polarized light. To derive the Brewster angle equation from the first element, we set the first element equal to zero and isolate for the angle of incidence.

$$\cos(\theta_I)(p_x \cos(\theta_I) - p_z \sin(\theta_I)) = 0 \quad (\text{S.21})$$

Simplification of equation S.21 defines a condition where the electric dipole does not reflect any light, which occurs when the tangent of the angle of incidence is equal to the ratio of the electric dipole moment along the x- and z-directions as seen below.

$$\tan(\theta_I) = \frac{p_x}{p_z} = n \quad (\text{S.22})$$

We note that  $p_x$  and  $p_z$  are complex numbers, as they are related to time varying electric fields. In order for equation S.22 to be satisfied, and for the Brewster angle to occur, these moments must be real numbers.

Furthermore,  $\text{atan}\left(\frac{p_x}{p_z}\right) = \tilde{\theta}_{ED} = \theta_{ED,r} + i\theta_{ED,i}$  is the angle of the complex electric dipole moment, which gives us a modified form of the Brewster angle condition.

$$\theta_{ED,r} - \theta_I + i\theta_{ED,i} = 0^\circ + 0i \quad (\text{S.23})$$

We obtain the traditional Brewster angle condition by realizing the angle of transmission is related to  $\theta_{ED,r}$  via a  $90^\circ$  rotation, as the direction of propagation and electric field are perpendicular to each other  $\theta_T = \theta_{ED,r} - 90^\circ$ . These angles are presented in Figure 1 in the main text.

$$\theta_I + \theta_T = 90^\circ \quad (\text{S.24})$$

Using equation S.24, we derive equation 1 from Snell's Law,  $\sin(\theta_I) = n \sin(\theta_T)$ , highlighting how equation S.22 is equal to the refractive index of the film.

$$\sin(\theta_I) = n \sin(\theta_I - 90^\circ) \quad (\text{S.25})$$

Simplifying this equation gives us the well-known Brewster angle equation with the relations,  $\sin(\theta_I - 90^\circ) = \cos(\theta_I)$  and  $\frac{\sin(\theta_I)}{\cos(\theta_I)} = \tan(\theta_I)$

$$\tan(\theta_B) = n \quad (\text{S.26})$$

## 2.2 Magnetic Dipole Brewster Angle

To derive the magnetic dipole Brewster angle, we begin with the vector describing the reflected light from the magnetic dipole.

$$\vec{m} \times \vec{n} = \begin{pmatrix} -m_y \cos(\theta_I) \\ -m_z \sin(\theta_I) + m_x \cos(\theta_I) \\ m_y \sin(\theta_I) \end{pmatrix} \quad (\text{S.27})$$

It should be clear that no p-polarized Brewster angle can exist as  $m_y \cos(\theta_I) \neq 0$ . Only an s-polarized Brewster angle can exist as  $-m_z \sin(\theta_I) + m_x \cos(\theta_I) = 0$  is possible. Re-arranging this equation we obtain the following.

$$\frac{m_x}{m_z} = \frac{\sin(\theta_I)}{\cos(\theta_I)} \quad (\text{S.28})$$

Which gives us an equation for the magnetic dipole Brewster angle presented in the main text.

$$\tan(\theta_I) = \frac{m_x}{m_z} \quad (\text{S.29})$$

## 2.3 Electric Quadrupole Brewster Angle

To derive the electric quadrupole Brewster angle, we begin with the vector describing the reflected light from the electric quadrupole.

$$\vec{n} \times (\vec{n} \times (\hat{E}Q\vec{n})) = \begin{pmatrix} \cos^2(\theta_I) \sin(\theta_I) (EQ_{xx} - EQ_{zz}) + \cos(\theta_I) (EQ_{xz} \cos^2(\theta_I) - EQ_{zx} \sin^2(\theta_I)) \\ EQ_{yx} \sin(\theta_I) + EQ_{xz} \cos(\theta_I) \\ \cos(\theta_I) \sin^2(\theta_I) (EQ_{zz} - EQ_{xx}) + \sin(\theta_I) (EQ_{zx} \sin^2(\theta_I) - EQ_{xz} \cos^2(\theta_I)) \end{pmatrix} \quad (\text{S.30})$$

It appears that both s-polarized and p-polarized cases can be zero. But we begin with the p-polarized case,  $\cos^2(\theta_I) \sin(\theta_I) (EQ_{xx} - EQ_{zz}) + \cos(\theta_I) (EQ_{xz} \cos^2(\theta_I) - EQ_{zx} \sin^2(\theta_I)) = 0$ . Realizing that  $EQ_{xz} = EQ_{zx}$ , we can re-arrange this equation we get the following.

$$\frac{\cos(\theta_I) \sin(\theta_I)^2}{\cos(\theta_I)^2 \sin(\theta_I) - \cos(\theta_I)^3} = -\frac{EQ_{xz}}{EQ_{xx} - EQ_{zz}} \quad (\text{S.31})$$

The left hand side of the above equation is related to the tan function through  $\frac{\cos(\theta_I) \sin(\theta_I)^2}{\cos(\theta_I)^2 \sin(\theta_I) - \cos(\theta_I)^3} = \frac{1}{2} \tan(2\theta_I)$ .

$$\tan(2\theta_I) = -\frac{2EQ_{xz}}{EQ_{xx} - EQ_{zz}} \quad (\text{S.32})$$

To derive the s-polarized Brewster angle we set  $EQ_{yx} \sin(\theta_I) + EQ_{xz} \cos(\theta_I) = 0$ . Re-arranging this equation we get.

$$\frac{\sin(\theta_I)}{\cos(\theta_I)} = \frac{EQ_{xz}}{EQ_{yx}} \quad (\text{S.33})$$

$$\tan(\theta_I) = \frac{EQ_{xy}}{EQ_{zy}} \quad (\text{S.34})$$

## 2.4 Magnetic Quadrupole Brewster Angle

$$\vec{n} \times (\hat{M}Q\vec{n}) = \begin{pmatrix} -\cos(\theta_I)(MQ_{yz} \sin(\theta_I) + MQ_{yz} \cos(\theta_I)) \\ \cos(\theta_I) \sin(\theta_I)(MQ_{xx} - MQ_{zz}) + MQ_{zx} \cos^2(\theta_I) - MQ_{zx} \sin^2(\theta_I) \\ \sin(\theta_I)(MQ_{yx} \sin(\theta_I) + MQ_{xz} \cos(\theta_I)) \end{pmatrix} \quad (\text{S.35})$$

As with the electric quadrupole, the magnetic quadrupole can support p- and s-polarized Brewster angles. To derive the p-polarized Brewster angle, we set  $-\cos(\theta_I)(M_{yx} \sin(\theta_I) + M_{yz} \cos(\theta_I)) = 0$ .

$$-\frac{MQ_{yx}}{MQ_{yz}} = \frac{\sin(\theta_I)}{\cos(\theta_I)} \quad (\text{S.36})$$

$$\tan(\theta_I) = -\frac{MQ_{xy}}{MQ_{zy}} \quad (\text{S.37})$$

For the s-polarized Brewster angle, we set  $\cos(\theta_I) \sin(\theta_I)(M_{xx} - M_{zz}) + M_{xz} \cos^2(\theta_I) - M_{zx} \sin^2(\theta_I) = 0$  and  $M_{xz} = M_{zx}$

$$\frac{\cos(\theta_I) \sin(\theta_I)}{\cos(\theta_I)^2 - \sin(\theta_I)^2} = -\frac{MQ_{xz}}{MQ_{xx} - MQ_{zz}} \quad (\text{S.38})$$

$$\tan(2\theta_I) = -\frac{2MQ_{xz}}{MQ_{xx} - MQ_{zz}} \quad (\text{S.39})$$

## 2.5 Analytical Equation Brewster Angle Equation for the s-Polarized Magnetic Dipole

In this section we derive an analytical equation for the MD BA, showing that it should be equivalent to the ED Brewster angle.

To derive an analytical equation for the magnetic dipole Brewster angle, we follow the same steps as those presented to derive the electric dipole Brewster angle in the main text.

To begin, we set the reflection coefficient of the s-polarized magnetic dipole coefficient to zero.

$$-m_z \sin(\theta_I) + m_x \cos(\theta_I) = 0 \quad (\text{S.40})$$

Then we separate the  $\theta_I$  and magnetic dipole moments terms.

$$\tan(\theta_I) = \frac{m_x}{m_z} \quad (\text{S.41})$$

Applying inverse tangent to this equation gives us the Brewster angle condition for the magnetic dipole.

$$\theta_{MD, real} - \theta_I + i\theta_{MD, imag} = 0^\circ + 0i \quad (\text{S.42})$$

Equation S.42 is the magnetic dipole equivalent of the Brewster angle condition derived in the main text. Equation S.42 can be substituted into Snell's Law to obtain an analytical equation for the magnetic dipole Brewster angle, which mirrors the electric dipole Brewster angle derived in the main text.

$$\theta_{MD} + \theta_I + i\theta_{MD, imag} = 0^\circ + 0i \quad (\text{S.43})$$

We obtain the Brewster angle condition by realizing the angle of transmission is related to  $\theta_{MD, real}$  via a  $90^\circ$  rotation, as the direction of propagation and magnetic field are perpendicular to each other  $\theta_T = \theta_{MD, real} - 90^\circ$ .

$$\theta_I + \theta_T = 90^\circ \quad (\text{S.44})$$

we now derive an analytical equation from Snell's Law,  $\sin(\theta_I) = n \sin(\theta_T)$ .

$$\sin(\theta_I) = n \sin(\theta_I - 90^\circ) \quad (\text{S.45})$$

Simplifying this equation gives us the well-known Brewster angle equation with the relations,  $\sin(\theta_I - 90^\circ) = \cos(\theta_I)$  and  $\frac{\sin(\theta_I)}{\cos(\theta_I)} = \tan(\theta_I)$

$$\tan(\theta_{B, MD}) = n \quad (\text{S.46})$$

Therefore, we can make the following connection for the MD Brewster angle.

$$\tan(\theta_B) = \frac{m_x}{m_z} = n \quad (\text{S.47})$$

## 2.6 Equivalency Between s-Polarized Magnetic Dipole and Electric Dipole Reflection Coefficients

In main text, it is shown that the s-polarized reflection coefficients of the magnetic dipole and electric quadrupole have the same magnitude, phase regardless of angle as well as having Brewster angles that occur at the same wavelength and angle.

To demonstrate why this occurs, we show how the magnetic dipole and electric quadrupole moments may become equal to each other under certain conditions that occur in thin films.

These conditions are as follows. The electric quadrupole toroidal term must be negligible, and the incident light must be purely s-polarized, so only the current density,  $\vec{J}$ , along the y-direction is non-zero,  $J_y \neq 0$ .

Under these circumstances the magnetic dipole moment remains the same.

$$\vec{m}_a = \frac{3ik_d}{2} \int_V \frac{j_1(k_dr)}{k_dr} (\vec{r} \times \vec{J})_a dV \quad (\text{S.48})$$

However, the electric quadrupole moment is simplified as the toroidal term is presumed zero.

$$\hat{Q}_{ab} = \frac{-ik_d}{2} \int_V \frac{j_1(k_dr)}{k_dr} (3(\vec{r}_a \vec{J}_b - \vec{J}_a \vec{r}_b) - 2(\vec{r}_a \cdot \vec{J}_b) \hat{U}_{ab}) dr \quad (\text{S.49})$$

For s-polarized light, the  $m_x$  and  $m_z$  are non-zero and their simplified forms are below.

$$\vec{m}_x = \frac{3ik_d}{2} \int_V \frac{j_1(k_dr)}{k_dr} (-zJ_y) dV \quad (\text{S.50})$$

$$\vec{m}_z = \frac{3ik_d}{2} \int_V \frac{j_1(k_dr)}{k_dr} (xJ_y) dV \quad (\text{S.51})$$

$\hat{Q}_{xy}$  and  $\hat{Q}_{zy}$  are non-zero.

$$\hat{Q}_{xy} = \frac{3ik_d}{2} \int_V \frac{j_1(k_dr)}{k_dr} xJ_y dr \quad (\text{S.52})$$

$$\hat{Q}_{zy} = \frac{3ik_d}{2} \int_V \frac{j_1(k_dr)}{k_dr} (-zJ_y) dr \quad (\text{S.53})$$

Given that the volumes that equations S.50-S.53 are integrated over the same, it is clear that the following moments are equal to each other,  $m_x = \hat{Q}_{xy}$  and  $m_z = \hat{Q}_{zy}$  as long as the conditions mentioned earlier are true.

Furthermore, the individual coefficients for s-polarized light are the same for both MD and EQ, explaining why the magnitude and phase of their reflection coefficients are the same.

$$-m_z \sin(\theta_I) + m_x \cos(\theta_I) = EQ_{zy} \sin(\theta_I) + EQ_{xy} \cos(\theta_I) \quad (\text{S.54})$$

### 3 Complex Angles

It is important to note that complex angles arise naturally from equation 2, as the multipole moments are related to the complex electric fields, where the imaginary part describes the time varying component of the field. To mathematically explain the relation between the imaginary angle and it's magnitude in the imaginary plane and connection to the real parts, we derive the relation from the complex electric dipole moment along the x and z directions used in the main text. Using trigonometric relations, we can describe the complex electric dipole moment along the x and z directions.

$$p_{x,r} + ip_{x,i} = |\vec{p}| \sin(\theta_{ED,r} + i\theta_{ED,i}) \quad (\text{S.55})$$

$$p_{z,r} + ip_{z,i} = |\vec{p}| \cos(\theta_{ED,r} + i\theta_{ED,i}) \quad (\text{S.56})$$

Using the trigonometric identities  $\sin(a+b) = \cos(b)\sin(a) + \cos(a)\sin(b)$ ,  $\cos(a+b) = \cos(b)\cos(a) - \sin(a)\sin(b)$ ,  $\cos(ia) = \cosh(a)$  and  $\sin(ia) = i\sin(a)$ . We can separate these equations into their real and imaginary parts.

$$p_{x,r} + ip_{x,i} = |\vec{p}| [\cosh(\theta_{ED,i}) \sin(\theta_{ED,r}) + i \sinh(\theta_{ED,i}) \cos(\theta_{ED,r})] \quad (\text{S.57})$$

$$p_{z,r} + ip_{z,i} = |\vec{p}| [\cosh(\theta_{ED,i}) \cos(\theta_{ED,r}) - i \sinh(\theta_{ED,i}) \sin(\theta_{ED,r})] \quad (\text{S.58})$$

Next, we define the magnitude of the electric dipole moment using the complex moments along the x and z directions.

$$|\vec{p}| = \sqrt{|p_x|^2 + |p_z|^2} \quad (\text{S.59})$$

This can be further expanded into the real and imaginary parts as below.

$$|\vec{p}| = \sqrt{|p_{x,r}|^2 - |p_{x,i}|^2 + |p_{z,r}|^2 - |p_{z,i}|^2 + 2(p_{x,r}p_{x,i} + p_{z,r}p_{z,i})} \quad (\text{S.60})$$

We note that  $p_{x,r}p_{x,i} = -p_{z,r}p_{z,i}$ , based on equations S.57 and S.58, which can then be simplified to only consider the magnitudes in the real and imaginary planes.

$$|\vec{p}| = \sqrt{|p_r|^2 - |p_i|^2} \quad (\text{S.61})$$

Using equations S.57 and S.58 we can describe the magnitude of the real and imaginary parts as follows.

$$|p_r|^2 = |p_{x,r}|^2 + |p_{z,r}|^2 = |p|^2 \cosh^2(\theta_{ED,i}) \quad (\text{S.62})$$

$$|p_i|^2 = |p_{x,i}|^2 + |p_{z,i}|^2 = |p|^2 \sinh^2(\theta_{ED,i}) \quad (\text{S.63})$$

From equations S.62 and S.63 we can define the imaginary angle in terms of the real, imaginary and total magnitudes of the electric dipole moment, demonstrating that the imaginary angle is related to the magnitude of the imaginary parts, i.e it is a "measure" of whether a vector is complex valued or not.

$$\theta_{ED,i} = \operatorname{arcsinh} \left( \frac{|p_i|}{|\vec{p}|} \right) = \operatorname{arccosh} \left( \frac{|p_r|}{|\vec{p}|} \right) \quad (\text{S.64})$$

We note that if  $|p_i| = 0$ , then  $\operatorname{arcsinh} \left( \frac{|p_i|}{|\vec{p}|} \right) = 0$  and the vector is in the real plane, hence  $|p_r| = |\vec{p}|$  and  $\operatorname{arccosh} \left( \frac{|p_r|}{|\vec{p}|} \right) = 0$ .

S.62 and S.63 can be substituted into equation S.61 to obtain the following relation for the total magnitude.

$$|\vec{p}| = |\vec{p}| \sqrt{\cosh^2(\theta_{ED,i}) - \sinh^2(\theta_{ED,i})} \quad (\text{S.65})$$

This is further simplified with the relation,  $\cosh^2(\theta_{ED,i}) - \sinh^2(\theta_{ED,i}) = 1$  to show that we can re-obtain the correct result for the magnitude of a complex vector.

$$|\vec{p}| = |\vec{p}| \quad (\text{S.66})$$

## 4 Differences Between Zero Reflection for Fabry Perot and Brewster Angle Effects

In the main text, two separate minima are presented, the Brewster angle and Fabry Perot modes and while it is possible to distinguish them by using equations 1 and S.74 or by changing polarization, in this section, we show how our multipole model distinguished the two.

To compare and contrast Fabry Perot and Brewster angle effects, we investigated the angle dependent reflection at 1834 nm in Figures S1, at these wavelengths we observed both Fabry Perot and Brewster angle modes, making these wavelengths ideal for study.

Beginning with 1834 nm in Figure S1. The Brewster angle is identified in all p-polarized datasets, Figures S1 (a) as the black line approximately at 64 degrees, this angle was calculated from equation 1 using the measured refractive index of our sample. The Fabry Perot modes, which are seen as regions of zero reflection in Figure S1 (a) and (b) at 20 degrees are marked by the magenta line. The regions of zero reflection match perfectly with the expected location of the 1st order Fabry Perot modes, which is calculated with equation S.74 below.

The usual Brewster angle is limited to p-polarized light, Figures S1 (a), (b) and (c). In Figure S1 (b), the ED reflection coefficient is zero,  $|r_{ED}| = 0$ , as the electric dipole moment and angle of incidence have aligned. The MD and EQ coefficients are equal to each other,  $|r_{MD}| = |r_{EQ}|$ . In Figure S1 (c), these two multipoles are destructively interfering as there is a  $\pi$  phase difference between them and therefore result in zero reflection,  $|r_{MD}| + |r_{EQ}| = 0$ .

In Figures S1 (b) and (e), the 1st order Fabry Perot mode is located at the angle where the sum of the MD and EQ coefficients are equal to the ED coefficient,  $|r_{MD}| + |r_{EQ}| = |r_{ED}|$  for both polarizations. For p-polarized light that is  $0.37 + 0.23 = 0.60$  and for s-polarized light that is  $0.35 + 0.35 = 0.70$ . Looking at the phase of these reflection coefficients in Figure S1 (c) and (f), the MD and EQ coefficients are constructively interfering with each other, while destructively interfering with the electric dipole, resulting in zero reflection,  $(|r_{MD}| + |r_{EQ}|) - |r_{ED}| = 0$ .

We have shown that both Fabry Perot and Brewster angles arise from the interference between different multipoles and satisfy the equation  $r_{MD} + r_{EQ} + r_{ED} = 0$ . But the nature of this interference effect is different.

In the case of the Fabry Perot mode it is the destructive interference between ED and MD/EQ multipoles that leads to zero reflection,  $(r_{MD} + r_{EQ}) - r_{ED} = 0$ . This matches a previous study of GaP thin films [2], where the same interference effect was

identified at normal incidence for the 1st order Fabry Perot mode, and we show this is true at non-zero angles as well.

For the Brewster angle, it is the destructive interference between MD and EQ that results in zero reflection, as well as the alignment of the electric dipole moment with the angle of incidence, so that  $(r_{MD} + r_{EQ}) = 0$ .

We note that if one were to only consider the reflection spectra and define the Brewster angle as the angle where the reflection is zero, then the Fabry Perot modes may be confused for Brewster angles, which may have already occurred in literature [4, 5]. In all of these cases, they defined the Brewster angle as the point where reflection was 0, but this is not sufficient to distinguish between Brewster angle and Fabry Perot modes, which we have demonstrated as distinctly different interference phenomena. Concerns about proper definitions of the Brewster angle have been highlighted previously [6].

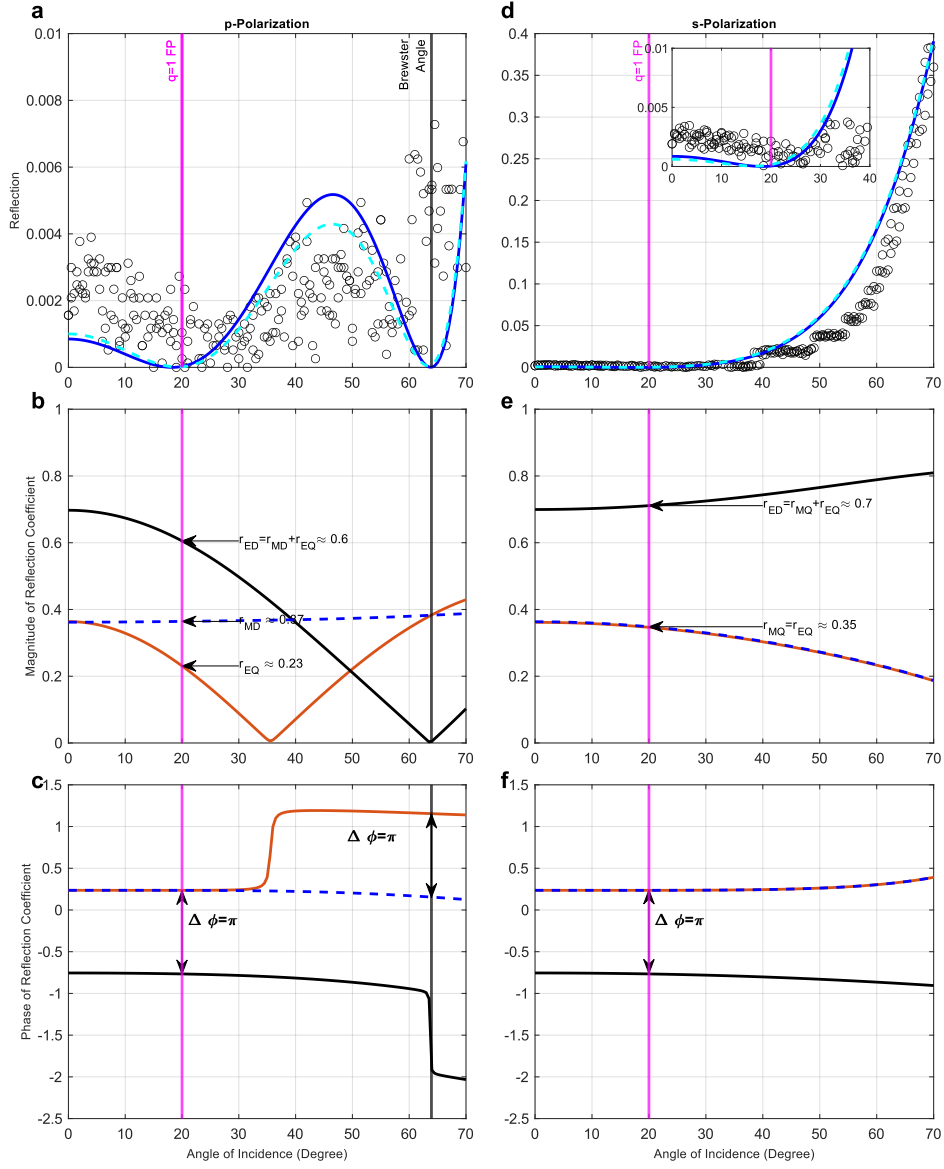


**Fig. S1** Reflection at 1834 nm. (a) p-Polarized reflection for measurement and simulations. (b) Magnitude of reflection coefficients for individual multipoles. (c) Phase of reflection coefficients for individual multipoles. (d)-(f) s-Polarized equivalent of (a)-(c)

## 5 SiN Ellipsometry

The refractive index of our  $\text{Si}_3\text{N}_4$  sample presented in the main text is presented in Table S1. The refractive index was extracted by fitting an absorbing Cauchy equation to the reflection of the thin film, which is shown below.

$$n(\lambda) = A + \frac{B}{\lambda^2} + \frac{C}{\lambda^3} \quad (\text{S.67}) \quad k(\lambda) = D + \frac{E}{\lambda^2} + \frac{F}{\lambda^3} \quad (\text{S.68})$$

The fitted parameters,  $A, B, C, D, E, F$  are described in the table below with their corresponding uncertainties.

**Table S1** Table of SiN fitting parameters extracted via ellipsometry.

Fitting Parameter	Measurement 1	Measurement 2
A	$+2.065 \times 10^{+0} \pm 9.851 \times 10^{-3}$	$+2.032 \times 10^{+0} \pm 2.074 \times 10^{-3}$
B	$+9.848 \times 10^{-3} \pm 1.429 \times 10^{-3}$	$+2.671 \times 10^{-2} \pm 2.520 \times 10^{-3}$
C	$+1.518 \times 10^{-3} \pm 1.046 \times 10^{-4}$	$+5.626 \times 10^{-5} \pm 1.954 \times 10^{-5}$
D	$+2.996 \times 10^{-3} \pm 4.695 \times 10^{-3}$	$-2.382 \times 10^{-2} \pm 1.116 \times 10^{-3}$
E	$-2.002 \times 10^{-3} \pm 4.116 \times 10^{-4}$	$+4.053 \times 10^{-2} \pm 2.344 \times 10^{-2}$
F	$+2.775 \times 10^{-4} \pm 3.448 \times 10^{-5}$	$+1.283 \times 10^{-5} \pm 1.575 \times 10^{-5}$

The difference between measurements 1 and 2 is the fitting method itself. In measurement 1 we assume a single layer, is a smooth thin film with no rough surface. Measurement 2 involved fitting with 3 layers, the smooth thin film as with measurement 1, but with two rough surfaces on either side, these layers are a 50/50 mix of air and SiN whose thicknesses were estimated to be 13 and 5 nm. However, both fittings produce the same thickness for the homogeneous SiN layer of  $455 \text{ nm} \pm 5 \text{ nm}$ . For simulations used in the main paper, we used the refractive indices of measurement 2 assuming that  $k(\lambda) = 0$ .

## 6 Importance of the Magnetic Dipole to the Brewster angle.

This can be demonstrated in Figure 6. We successively add multipoles to our reflection model in equation 2. only considering the electric dipole, the black line, produces the Brewster angle, but has poor agreement at smaller angles. Introducing the magnetic dipole, the dashed blue line, introduces large error and the Brewster angle disappears. It is only upon adding the electric quadrupole, orange dashed line, that the Brewster angle is re-obtained, with excellent agreement at all other angles.

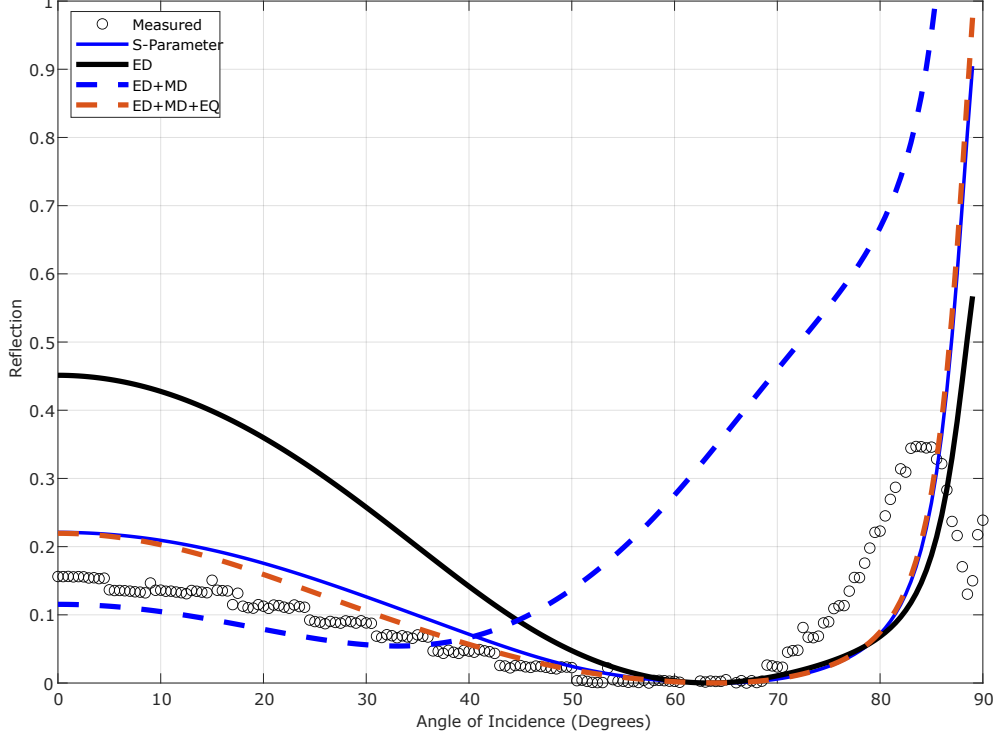


**Fig. S2** Demonstration of the importance of magnetic dipole and electric quadrupole in observing the Brewster angle. Dashed lines represent the multipole model, equation 2, with different multipole contributions. black (ED), dashed blue (ED+MD) and dashed orange (ED+MD+EQ). Good agreement between the multipole model and s-parameter (blue line)/ measurement (black circle) only occurs when all three multipoles are accounted for.

## 7 Pseudo-Brewster Angle

Another phenomenon that is associated with angular reflection from thin-films is the Pseudo-Brewster angle [7, 8]. The angle occurs for sufficiently lossy media with complex refractive index,  $n + ik$ , where the absorption of the media is defined by  $k = \frac{\alpha\lambda}{4\pi}$  [9], where  $\alpha$  is the absorption coefficient, which is typically seen the vicinity of a bandgap of a semiconductor such as silicon, or in conductive material such as gold. In this case, the zero in reflection is replaced with a non-zero reflection minimum. To ascertain the nature of this phenomena, we investigated a SiN film at 2000 nm as above, but now setting  $k=0$  and artificially  $k=2$  as seen in Figure S3.

In Figure S3 (a), we show the features of the Pseudo-Brewster angle for p-polarized incident light, the non-zero reflection minimum, the minimum value of this reflection and its angular location increases as we increase  $k$ .

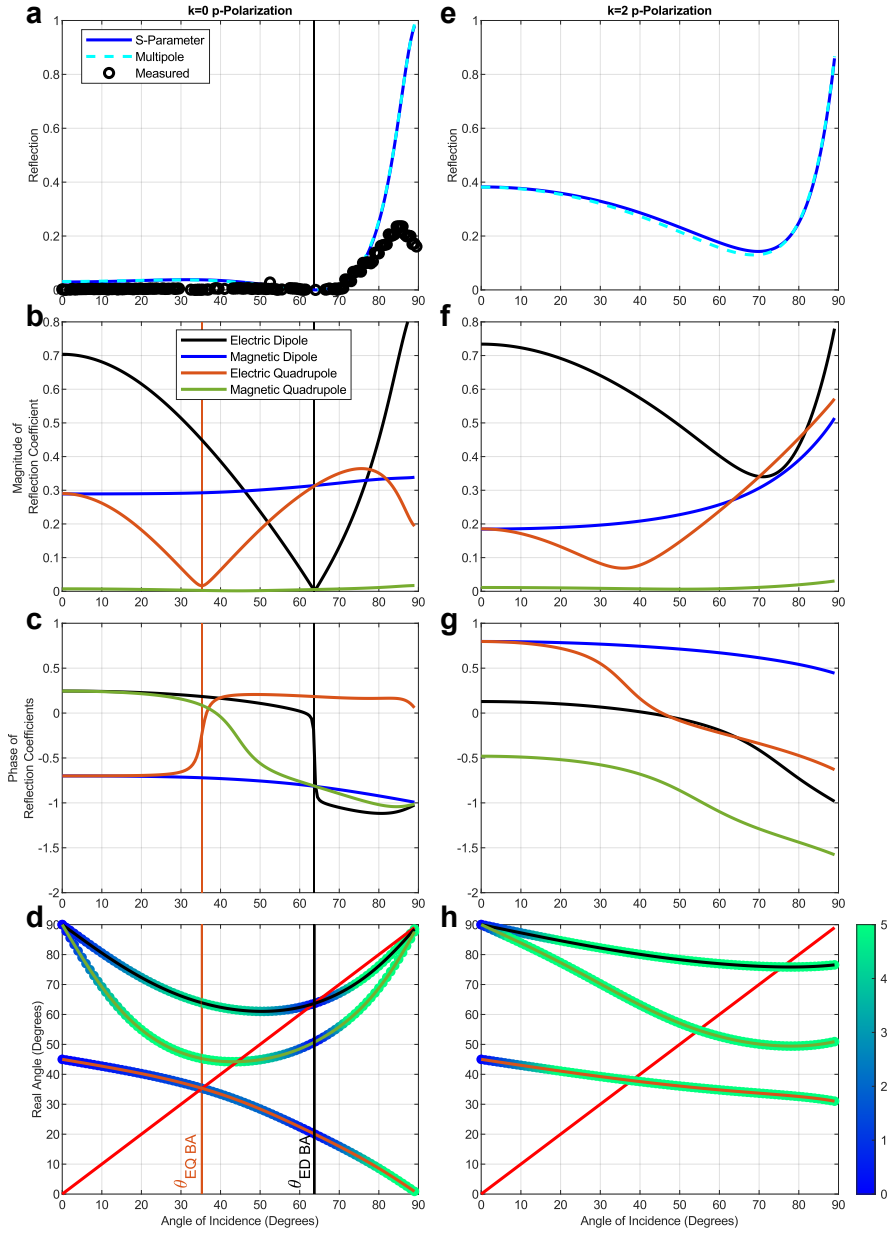


**Fig. S3** Investigation of the p-polarized Pseudo-Brewster angle using our multipole model. The Brewster angle in lossless media,  $n=2+0i$  (a)-(d) is compared to a lossy media with  $n=2+2i$  (e)-(h) at 2000 nm using the thickness of our SiN thin film, 455 nm. (a) and (e) Reflection for  $k=0$  and 2. (b) and (f) Magnitude of individual reflection coefficients for  $k=0$  and 2. (d) and (h) Phase of reflection coefficient of individual reflection coefficients for  $k=0$  and 2. (c) and (g) Phase of reflection coefficient of individual reflection coefficients for  $k=0$  and 2. (d) and (h) Angle of multipoles for lossless (d) and lossy (h) material.

As shown previously, the magnitude of the electric dipole reflection coefficient is zero at the Brewster angle, however in Figure S3 (b), this is not true for  $k=2$ , suggesting that the electric dipole moment is not aligning with the angle of incidence. In addition, the destructive interference between MD and EQ, plotted in Figure S3 (c) as the phase difference between their reflection coefficients, shows that complete destructive interference does not occur at the reflection minimum when introducing loss. In figure S3 (d) and (h) we investigate the alignment between multipoles. It is seen that while the  $k=2$  electric dipole angle aligns in the real plane, the imaginary part is non-zero, demonstrating that the Brewster angle condition is not satisfied when loss is introduced. From this analysis we can clearly show that the Pseudo-Brewster angle is not a true Brewster angle, and the name is therefore appropriate.

## 8 Measuring Transmission

This section outlines the design of experiment and methodology to measure transmission, which is used to calculate the reflection presented in the main text, assuming that in the spectral region from 750 to 2200 nm that absorption is zero.

In order to measure the transmission through SiN thin films, the set up outlined in Figure S4 (a) was constructed with parts sourced from Thorlabs, for comparison with our multipole and S-parameter models. The light source was a tungsten halogen light source (SLS201L/M), which is connected to a multi-mode fiber cable (M15L01) and collimator (F110SMA-1550) to create the incident beam. A Glan Thompson polarizer (GTH10M) is used to polarize the beam. The rotational stage (K10CR2) supports the sample holder (PC2/M), which is joined to the rotational stage with a combination of parts (SM1L10). An iris (ID20/M) was placed to reduce the size of the beam after transmission. A lens (AC254-050-A-ML) is then used to focus the light onto a fiber cable connected to a spectrometer. Two separate spectrometers are used to measure transmission from 400-1000 nm and 1000-2200 nm, both are Ocean Optic Spectrometers. To take measurements, a MATLAB script was written to control the rotational motor and spectrometers. Control over the rotation motor was provided by [10].

To correctly calibrate the setup outlined in Figures S4 (a), 2 steps are outlined in Figure S4 (b) and (c). The first step outlined in Figure S4 (b), to know the true angle of incidence/incidence, we search for the  $\pm 90$ -degree angle of incidence. This can be found by matching the shadow of the sample with a bright fringe resulting from the near perfect reflection seen in all films towards 90 degrees. An angle of incidence of 90 degrees is obtained when this bright fringe disappears or overlaps with the shadow of the sample, this fringe and shadow are shown in Figure S6.

Step 2 is outlined in Figure S4 (c). The possibility remains that the sample is not aligned with the centre of rotation of the motor. This will be observable when rotating the sample between  $\pm 90$  degrees, as the shadow of the sample will be laterally displaced. The centre of rotation will lie in between the position of the two shadows at  $\pm 90$  degrees and will be the region where the sample shadow must be moved to.

If steps 1 and 2 have been performed correctly, mirror symmetry through an angle of incidence of 0 when measuring reflection, as seen in Figure S4 is observed. Ensuring

that the Brewster angle appears at the same angle in both positive and negative directions may assist this calibration.

The reference measurement that accounts for optical losses in the setup, is presented in Figure S4 (b). It is the ratio of the measured intensity from the sample and the reference intensity without the sample that gives us measured reflection in Figure S4 (c). The dark current of the spectrometers are automatically accounted for in these measured intensities.

Very large angles have major issues as the corners play a non-negligible role in the measured transmission, making observation of the Fabry Perot modes at large angles difficult. This is seen at very large angles in Figure S7(c), with the large red regions, which suggest large values of reflection from the SiN surface, when in reality, it is the reflection from the corners of the sample where the Si frame of the sample is located.

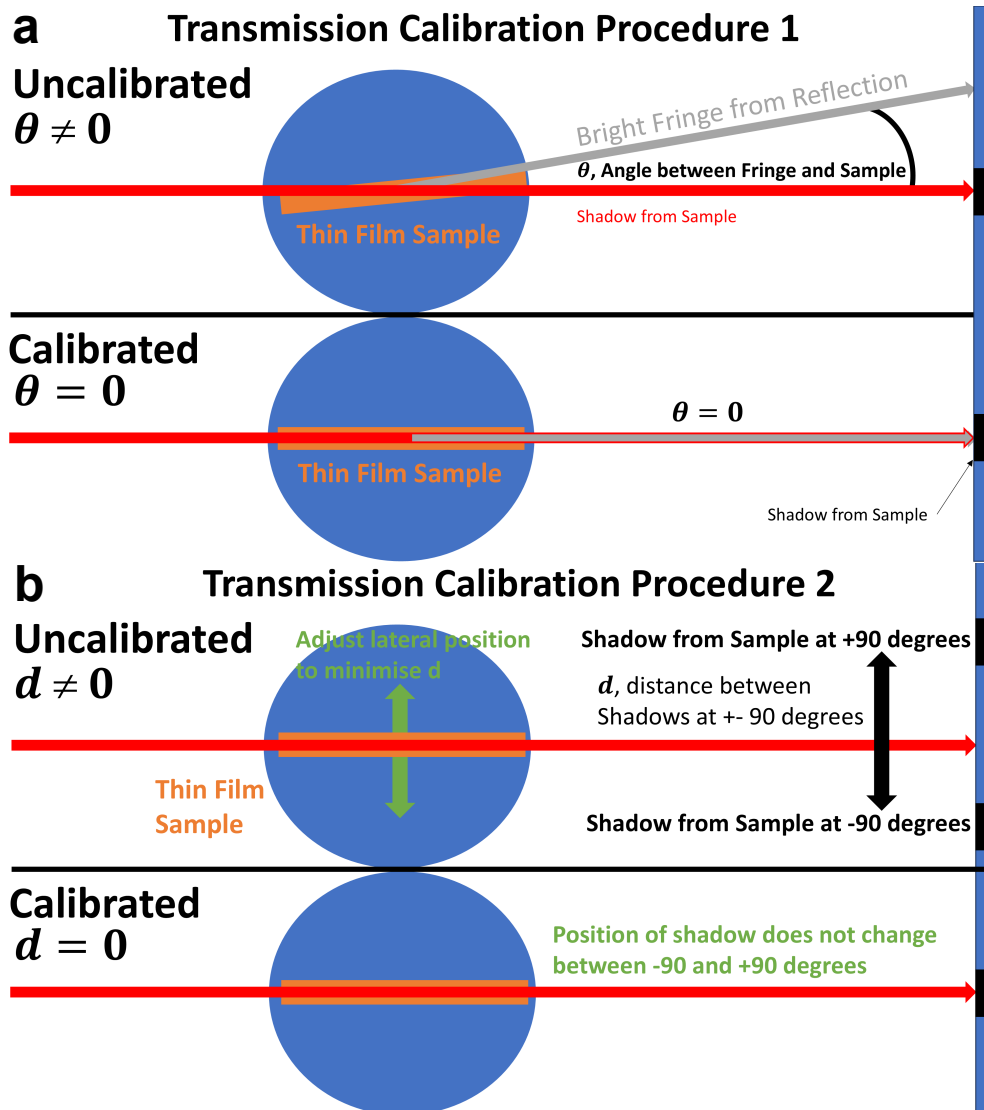


**Fig. S4** (a) First procedure to calibrate the angle of incidence. The overlap between the bright fringe resulting from reflection (grey arrow) and the shadow (red arrow after sample) corresponds an angle of zero between the shadow and fringe, which corresponds to an angle of incidence of 90 degrees between the sample and incident beam. (b) Second calibration procedure to reduce the mismatch between the centre of the sample and the centre of rotation.

To achieve reliable transmission measurements approaching glancing angles, i.e. towards 90 degrees angle of incidence, a highly divergent beam is recommended for the following reasons.

Firstly, there will always be a ray passing through the centre of the rotation of the motor, and hence the beam will not “run off” the surface as we change the angle of incidence.

Secondly, as the sample is rotated towards larger angles, the surface area of the sample exposed to the beam is reduced, and the corners are exposed to the incident beam. The reflection and transmission of the corners will affect the measured transmission obscuring the transmission of the thin film.

If the sample’s surface area is significantly smaller than the beam diameter, one will measure a signal from both the sample surface, but also free space and the sample corners, reducing the accuracy of the measured transmission. This issue with large angles of incidence is demonstrated below in Figure S5. Further optimization at larger angles is feasible by increasing the distance between the iris and sample, or using a magnifying lens placed in-between iris and sample.

This is a desirable situation as it makes alignment of the beam with the set up significantly easier and is a critical consideration in the calibration procedures required for an accurate measurement of transmission, as will be shown in the following discussion.

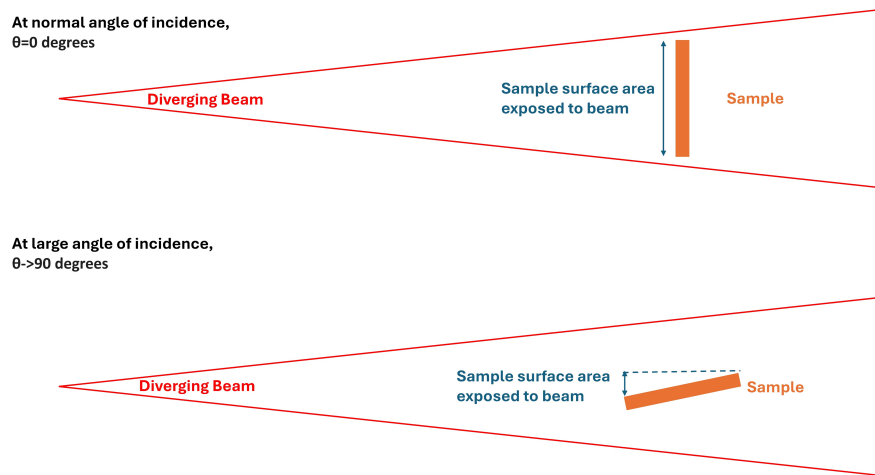


**Fig. S5** Issue with measurements at very large angles. Surface area exposed is reduced and corners dramatically affect measurements as the angle of incidence increases. While the surface is fully illuminated at all angles, the corners are illuminated more as the angle of incidence increases.

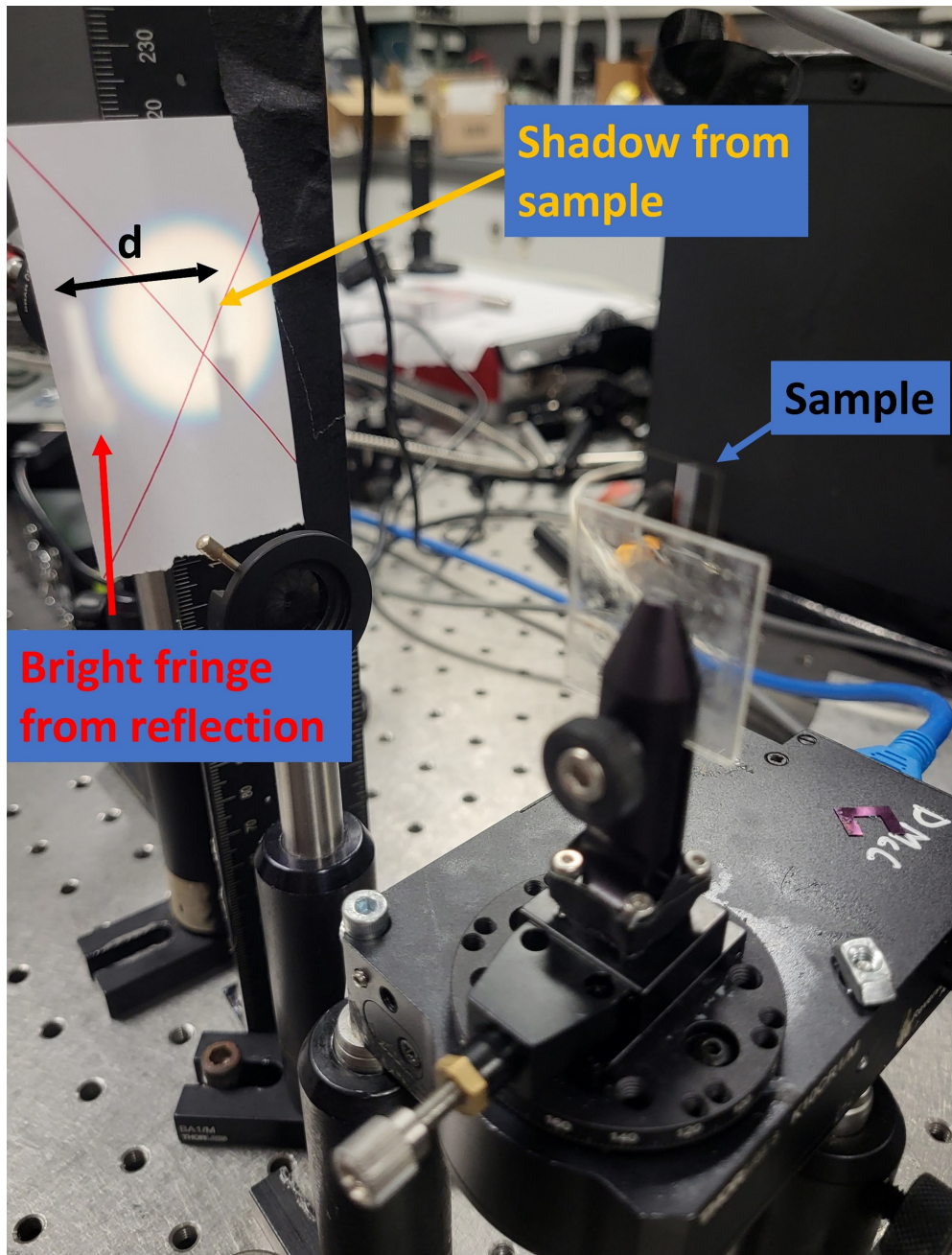


**Fig. S6** Image of set up in Figure S4 (a) with various parts labeled. SiO<sub>2</sub> sample is shown for demonstrative purposes.

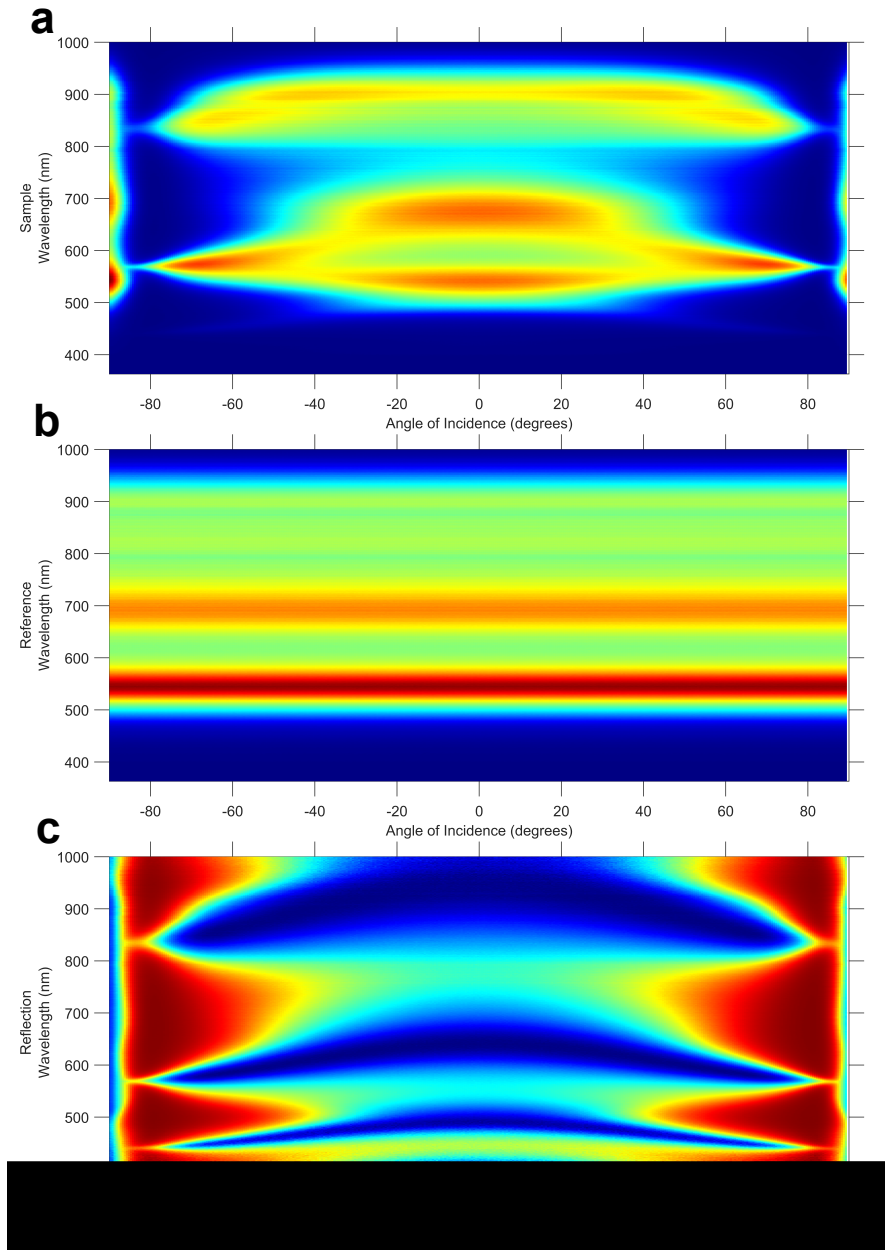


**Fig. S7** Example of verified measurement after steps outlined in Figure S4 for p-polarized light in the visible spectrum. (a) Measured intensity from SiN sample. (b) Measured intensity used for reference, i.e intensity in the absence of SiN sample. (c) Reflection, calculated from measured transmission, which is the produced by dividing subplot (a) by subplot (c), then subtracted from 1, assuming absorption is zero.

## 9 Fabry Perot Derivation

This section outlines the derivation of the angle dependence of Fabry Perot modes, which is plotted as a magenta line in the main text, Figures 4 and 5. Our initial derivation follows a standard textbook definition [11], however angle dependence of the Fabry Perot mode is introduced.

$$\lambda_q = \frac{2nd}{q} \quad (\text{S.69})$$

The above equation defines the wavelengths at which a Fabry Perot mode of  $q$  th order may exist at, for a refractive index  $n$  and film thickness  $d$ , but suggests no angle dependence in these modes. The solution to introduce angle dependence into the equation is to change the thickness,  $d$ , to the optical path length in the thin film,  $d_{OP}$ .

$$\lambda_q = \frac{2nd_{OP}}{q} \quad (\text{S.70})$$

At normal incidence, this matches the thickness of the film but will vary with angle. The optical path length will depend on the angle of transmission in the thin film and the thickness of the film, which depends on Snell's law.

$$\sin(\theta_I) = n \sin(\theta_T) \quad (\text{S.71})$$

This can be re-arranged as follows.

$$\theta_T = \sin^{-1} \left( \frac{\sin(\theta_I)}{n} \right) \quad (\text{S.72})$$

Now the optical path length can be defined in terms of the thickness and angle of transmission as follows.

$$d_{OP} = d \cos(\theta_T) = d \cos \left( \sin^{-1} \left( \frac{\sin(\theta_I)}{n} \right) \right) \quad (\text{S.73})$$

Substituting this into equation S.70 we obtain

$$\lambda_q = \frac{2nd \cos \left( \sin^{-1} \left( \frac{\sin(\theta_I)}{n} \right) \right)}{q} \quad (\text{S.74})$$

## References

- [1] Terekhov, P.D., Babicheva, V.E., Baryshnikova, K.V., Shalin, A.S., Karabchevsky, A., Evlyukhin, A.B.: Multipole analysis of dielectric metasurfaces composed of nonspherical nanoparticles and lattice invisibility effect. *Physical Review B* **99** (2019) <https://doi.org/10.1103/PhysRevB.99.045424>
- [2] Li, J., Papasimakis, N., MacDonald, K.F., Zheludev, N.I. Optical magnetic response without metamaterials. *APL Photonics* **6** (2021) <https://doi.org/10.1063/5.0054752>

- [3] Sreekanth, K.V., ElKabbash, M., Medwal, R., Zhang, J., Letsou, T., Strangi, G., Hinczewski, M., Rawat, R.S., Guo, C., Singh, R.: generalized Brewster Angle Effect in Thin-Film Optical Absorbers and Its Application for Graphene Hydrogen Sensing. *ACS Photonics* **6**(7), 1610–1617 (2019) <https://doi.org/10.1021/acsp Photonics.9b00564> .
- [4] Gan, M., Hanafusa, H., Kadoya, Y.: Experimental investigation on generalized Brewster effect for s-polarized terahertz waves at planar si-air interfaces with a thin doped layer. *Optics Express* **33**, 9306–9316 (2025) <https://doi.org/10.1364/OE.550968>
- [5] Ding, L., Qiu, T., Zhang, J., Wen, X.: Generalized Brewster effect tuned optically in a graphene/substrate system. *Journal of Optics* **21**(12), 125602 (2019) <https://doi.org/10.1088/2040-8986/ab4fa1>
- [6] Lakhtakia, A.: Would brewster recognize today’s brewster angle? *Optics News* **15**(6), 14–18 (1989) <https://doi.org/10.1364/ON.15.6.000014>
- [7] Azzam, R.M.A.: Fresnel’s interface reflection coefficients for the parallel and perpendicular polarizations: global properties and facts not found in your textbook. *Polarization Analysis and Measurement II*, vol. 2265 (1994). <https://doi.org/10.1117/12.186660>
- [8] Azzam, R.M.A., Thonn, T.F.: Pseudo-Brewster and second-Brewster angles of an absorbing substrate coated by a transparent thin film. *Appl. Opt.* **22**(24), 4155–4165 (1983) <https://doi.org/10.1364/AO.22.004155>
- [9] Fox, M.: *Optical Properties of Solids* vol. 70, p. (2001). <https://doi.org/10.1119/1.1691372>
- [10] Driver for Thorlabs BBD302/PRM1Z8/K10CR1 motorized stages. <https://uk.mathworks.com/matlabcentral/fileexchange/102234-driver-for-thorlabs-bbd302-prm1z8-k10cr1-motorized-stages>. Accessed: 2025-08-18
- [11] Bahaa E. A. Saleh, M.C.T.: 9. Resonator Optics, pp. 310–341. John Wiley & Sons, Ltd, (1991). <https://doi.org/10.1002/0471213748.ch9> . <https://onlinelibrary.wiley.com/doi/abs/10.1002/0471213748.ch9>